Compression Response of a Rapid-Strengthening Ultra-High Performance Concrete Formulation

September 2012

NTIS Accession No. PB2012-112545

FHWA Publication No. FHWA-HRT-12-065

U.S. Department of Transportation
Federal Highway Administration

FOREWORD

With the ever increasing congestion and deterioration of our nation's highway system, a need exists to develop highly durable and rapidly constructed infrastructure systems. Durable bridge structures that would require less intrusive maintenance and would exhibit longer life spans thus maximizing the use of the facility are highly desirable. Expediting bridge construction can minimize traffic flow disruptions. Ultra-high performance concrete (UHPC) is an advanced construction material which affords new opportunities to envision the future of the highway infrastructure. The Federal Highway Administration has been engaged in research on the optimal uses of UHPC in the highway bridge infrastructure since 2001 through its Bridge of the Future initiative. This report presents results of a study aimed at assessing the setting and early age compressive mechanical response of a rapid-strengthening UHPC formulation. The accelerated achievement of particular mechanical response benchmarks is of particular interest as it could enable broader use of UHPC-class materials in accelerated bridge construction projects.

This report corresponds to the TechBrief titled "Compression Response of a Rapid-Strengthening Ultra-High Performance Concrete Formulation" (FHWA-HRT-12-064). This report is being distributed through the National Technical Information Service for informational purposes. The content in this report is being distributed "as is" and may contain editorial or grammatical errors.

TECHNICAL REPORT DOCUMENTATION PAGE

1. Report No. FHWA-HRT-12-065	2. Government Accession No. NTIS PB2012-112545	3. Recipient's Catalog No.
4. Title and Subtitle Compression Response of a Rapid-Strengthening Ultra-High Performance Concrete Formulation		5. Report Date September 2012 6. Performing Organization Code:
7. Author(s) Benjamin A. Graybeal and Brenton Stone		8. Performing Organization Report No.
9. Performing Organization Name and Address Office of Infrastructure Research & Development Federal Highway Administration 6300 Georgetown Pike McLean, VA 22101-2296		10. Work Unit No. 11. Contract or Grant No.
12. Sponsoring Agency Name and Address Office of Infrastructure Research & Development Federal Highway Administration 6300 Georgetown Pike McLean, VA 22101-2296		13. Type of Report and Period Covered 14. Sponsoring Agency Code HRDI-40

15. Supplementary Notes

The research discussed herein was completed at the Turner-Fairbank Highway Research Center. Portions of the work were completed by Global Consulting, Inc. under contract DTFH61-07-C-00011. Brenton Stone of Global was the co-Prinicipal Investigator on this project with Benjamin Graybeal who leads the FHWA Structural Concrete Research Program.

16. Abstract

Compressive mechanical properties are critical indicators of the degree of hydration of concrete and are frequently used as indicators of other mechanical and durability properties. The rate of compressive mechanical response development is of importance to construction projects wherein the concrete hydration is on the critical path. Ultra-high performance concrete (UHPC), when used in field-cast connections between prefabricated bridge elements, can create robust connections which emulate monolithic components. Traditional UHPC formulations tend to express a delay prior to setting and initial mechanical property development. This research program investigated the compressive mechanical response of a new UHPC formulation intended for use in field-cast infrastructure connections. The time to initiation and rate of property development was observed to be influenced by the ambient environment surrounding the concrete during curing. At an elevated curing temperature, the UHPC was observed to reach 10 ksi compressive strength at 11 hours. The compressive strength, modulus of elasticity, axial strain at peak strength, and overall stress-strain response were captured under three curing conditions from early age through 56 days after casting.

This report corresponds to the TechBrief titled "Compression Response of a Rapid-Strengthening Ultra-High Performance Concrete Formulation" (FHWA-HRT-12-064).

17. Key Words	18. Distribution Statement
Ultra-high performance concrete, UHPC, fiber-reinforced concrete, bridges, accelerated construction, compressive strength gain, modulus of elasticity	No restrictions. This document is available through the National Technical Information Service, Springfield, VA 22161.

19. Security Classif. (of this report)	20. Security Classif. (of this page)	21. No. of Pages	22. Price
Unclassified	Unclassified	66	N/A

Form DOT F 1700.7 (8-72) Reproduction of completed page authorized

SI* (MODERN METRIC) CONVERSION FACTORS

APPROXIMATE CONVERSIONS TO SI UNITS

Symbol	When You Know	Multiply By	To Find	Symbol
		LENGTH		
in	inches	25.4	millimeters	mm
ft	feet	0.305	meters	m
yd	yards	0.914	meters	m
mi	miles	1.61	kilometers	km
		AREA		
in^2	square inches	645.2	square millimeters	mm^2
ft^2	square feet	0.093	square meters	m^2
yd^2	square yard	0.836	square meters	m^2
ac	acres	0.405	hectares	ha
mi^2	square miles	2.59	square kilometers	km^2
		VOLUME		
fl oz	fluid ounces	29.57	milliliters	mL
gal	gallons	3.785	liters	L
ft^3	cubic feet	0.028	cubic meters	m^3
yd^3	cubic yards	0.765	cubic meters	m^3
	NOTE: volumes greater than 1000 L shall be shown in m^3			
		MASS		
oz	ounces	28.35	grams	g
lb	pounds	0.454	kilograms	kg
T	short tons (2000 lb)	0.907	megagrams (or "metric ton")	Mg (or "t")
		TEMPERATURE (exact degrees)		
^oF	Fahrenheit	5 (F-32)/9 or (F-32)/1.8	Celsius	^oC
		ILLUMINATION		
fc	foot-candles	10.76	lux	lx
fl	foot-Lamberts	3.426	$candela/m^2$	cd/m^2
		FORCE and PRESSURE or STRESS		
lbf	poundforce	4.45	newtons	N
lbf/in^2	poundforce per square inch	6.89	kilopascals	kPa

APPROXIMATE CONVERSIONS FROM SI UNITS

Symbol	When You Know	Multiply By	To Find	Symbol
		LENGTH		
mm	millimeters	0.039	inches	in
m	meters	3.28	feet	ft
m	meters	1.09	yards	yd
km	kilometers	0.621	miles	mi
		AREA		
mm^2	square millimeters	0.0016	square inches	in^2
m^2	square meters	10.764	square feet	ft^2
m^2	square meters	1.195	square yards	yd^2
ha	hectares	2.47	acres	ac
km^2	square kilometers	0.386	square miles	mi^2
		VOLUME		
mL	milliliters	0.034	fluid ounces	fl oz
L	liters	0.264	gallons	gal
m^3	cubic meters	35.314	cubic feet	ft^3
m^3	cubic meters	1.307	cubic yards	yd^3
		MASS		
g	grams	0.035	ounces	oz
kg	kilograms	2.202	pounds	lb
Mg (or "t")	megagrams (or "metric ton")	1.103	short tons (2000 lb)	T
		TEMPERATURE (exact degrees)		
^oC	Celsius	1.8C+32	Fahrenheit	^oF
		ILLUMINATION		
lx	lux	0.0929	foot-candles	fc
cd/m^2	$candela/m^2$	0.2919	foot-Lamberts	fl
		FORCE and PRESSURE or STRESS		
N	newtons	0.225	poundforce	lbf
kPa	kilopascals	0.145	poundforce per square inch	lbf/in^2

*SI is the symbol for the International System of Units. Appropriate rounding should be made to comply with Section 4 of ASTM E380.
(Revised March 2003)

TABLE OF CONTENTS

LIST OF FIGURES

LIST OF TABLES

CHAPTER 1. INTRODUCTION

INTRODUCTION

Highway infrastructure in the United States is aging and is sometimes incapable of adequately accommodating the volume of traffic loads. Most of the roads and bridges traveled by the public each day were designed and constructed decades ago, and these assets are in need of maintenance and rehabilitation in order to maintain an appropriate level of service. So as to keep the interruptions to the traveling public at a minimum, many transportation projects are specifying the deployment of rapid construction practices when rehabilitating existing infrastructure.

One example of this practice is known as accelerated bridge construction (ABC). One commonly deployed concept within ABC is to prefabricate significant portions of the new bridge structure offsite, then assemble and connect them onsite during an expedited construction timeframe. Precast concrete elements can provide significant benefit, as they can be designed to replace conventional cast-in-place concrete construction, thus removing the curing process from the construction schedule and expediting the completion of the rehabilitation.

However, the use of prefabricated bridge elements can necessitate the use of field-applied connections between these elements. These connections must be completed rapidly and must be sufficiently robust so as to not create a weak point within the finished structure. Field-cast concrete or other cementitious material connections have been applied countless times over recent decades. Critical aspects of these connections include the rate of mechanical property development, the dimensional stability, and the durability of the field-cast materials. These connections have frequently required complex designs, thus limiting their constructability and thus their use. When deployed, the connection systems have sometimes underperformed, resulting in reduced serviceability of the finished structure.

Ultra-high performance concrete (UHPC) is a relatively new class of cementitious composite materials which has been developed in recent decades. Research and field deployments of UHPC have demonstrated that this concrete is appropriate for use in field-cast connections between prefabricated bridge elements.[1,2] The advanced mechanical and durability properties of UHPC facilitate the design of simple connections which cease to be weak points within the finished structure.

The intent of this research project is to assess the compressive mechanical response of a new formulation of a UHPC. The material utilized in this research was a rapid-strengthening blend of UHPC (UHPC-RS). While conventional UHPC is still a relatively new construction material, this particular rapid-strengthening blend of UHPC only became available recently. The inherent ability of this concrete to more rapidly gain strength, potentially combined with externally accelerated curing, could increase the use of rapid-strengthening UHPC in ABC projects in coming years.

OBJECTIVE

The objective of this research study was to evaluate the compressive mechanical response of a rapid strengthening UHPC exposed to a range of curing conditions.

SUMMARY OF APPROACH

The research discussed herein focuses on the assessment of compressive mechanical response of a rapid-strengthening UHPC material to be used in structural applications. In order to assess the performance of this UHPC-RS, batches utilizing the same mixture design were mixed and used to cast 3-in. diameter, 6-in. nominal length cylinders to be tested in uniaxial compression until failure. A second mixture design was developed and tested which contained an additional chemical admixture. Variables considered within the study included the age since blending of the UHPC-RS premix powder, the effect of using a chemical accelerator, and the effect of curing temperature on the compressive mechanical response.

OUTLINE OF REPORT

This report is divided into six chapters. Chapters 1 and 2 provide an introduction to the research and provide background information useful to understanding this study's results. Chapter 3 presents the mixing, casting, and specimen testing details. Where Chapter 4 presents tables and graphs detailing the test results, Chapter 5 presents a discussion of the results and associated analyses. Finally, Chapter 6 presents the conclusions and recommendations garnered from the results of this research.

CHAPTER 2. BACKGROUND

INTRODUCTION

The contents of this chapter include a definition of ultra-high performance concrete (UHPC) and material details specific to this class of cementitious material. Additionally, information derived from other research projects that have used UHPC and tested the compressive mechanical responses is also presented.

ULTRA-HIGH PERFORMANCE CONCRETE

UHPC is a term that represents a class of a high-performance, fiber-reinforced, advanced cementitious composites. UHPC has been defined as follows:

> *UHPC is a cementitious composite material composed of an optimized gradation of granular constituents, a water-to-cementitious materials ratio less than 0.25, and a high percentage of discontinuous internal fiber reinforcement. The mechanical properties of UHPC include compressive strength greater than 21.7 ksi (150 MPa) and sustained post-cracking tensile strength greater than 0.72 ksi (5 MPa).[†] UHPC has a discontinuous pore structure that reduces liquid ingress, significantly enhancing durability compared to conventional concrete.*[(1,2)]

The advantages to using UHPC in place of a conventional concrete include advanced material properties such as noteworthy compressive strength, increased ductility due to steel fiber reinforcement, and superior durability characteristics because of a low water-cementitious material ratio (w/cm).

Unlike conventional concrete materials, this UHPC formulation contains no coarse aggregate. The mixture composition includes a pre-blended powder, or premix, and 0.5-in. (12.7-mm) long steel fibers. The premix is comprised of an optimized gradation of the following four materials: fine sand, portland cement, ground quartz, and silica fume. The silica fume particles fill tiny voids, or interstitial spaces, between the sand, quartz, and portland cement particles.

UHPC has been commercially available for more than a decade in the U.S.; however, the associated knowledge base required for effective design and deployment is just beginning to coalesce. Due to the significant compressive strengths achievable by UHPC materials, much of the published research has focused on that parameter.[(3,4,5)] There have been other recent research

[†]The tensile behavior of UHPC is generally defined as "strain-hardening," which is a broad term defining concretes wherein the sustained post-cracking strength provided by the fiber reinforcement is greater than the cementitious matrix cracking strength. However, the definitional dependence on cementitious matrix cracking strength may inappropriately include some concretes that exhibit low first-cracking strengths. Note that the post-cracking tensile strength and strain capacity of UHPC is highly dependent on the type, quantity, dispersion, and orientation of the internal fiber reinforcement.

projects that have investigated a wide range of material properties assisting in characterizing the material and thus further increasing the likelihood of more widespread use. The results compiled in Table 1 present average values for a number of test parameters relevant to the use of UHPC as obtained from independent testing of a commercially available product.[3]

Table 1. Typical field-cast UHPC material properties.

Material Characteristic	Average Result
Density	2,480 kg/m^3 (155 lb/ft^3)
Compressive Strength (ASTM C39; 28-day strength)	126 MPa (18.3 ksi)
Modulus of Elasticity (ASTM C469; 28-day modulus)	42.7 GPa (6200 ksi)
Split Cylinder Cracking Strength (ASTM C496)	9.0 MPa (1.3 ksi)
Prism Flexure Cracking Strength (ASTM C1018; 305-mm (12-in.) span)	9.0 MPa (1.3 ksi)
Mortar Briquette Cracking Strength (AASHTO T132)	6.2 MPa (0.9 ksi)
Direct Tension Cracking Strength (Axial tensile load)	5.5–6.9 MPa (0.8–1.0 ksi)
Prism Flexural Tensile Toughness (ASTM C1018; 305-mm (12-in.) span)	I_{30} = 48
Long-Term Creep Coefficient (ASTM C512; 77 MPa (11.2 ksi) load)	0.78
Long-Term Shrinkage (ASTM C157; initial reading after set)	555 microstrain
Total Shrinkage (Embedded vibrating wire gage)	790 microstrain
Coefficient of Thermal Expansion (AASHTO TP60–00)	14.7 x10^{-6} mm/mm/ºC (8.2 x10^{-6} in./in./ºF)
Chloride Ion Penetrability (ASTM C1202; 28-day test)	360 coulombs
Chloride Ion Permeability (AASHTO T259; 12.7-mm (0.5-in.) depth)	< 0.06 kg/m^3 (< 0.10 lb/yd^3)
Scaling Resistance (ASTM C672)	No Scaling
Abrasion Resistance (ASTM C944 2x weight; ground surface)	0.73 grams lost (0.026 oz. lost)
Freeze-Thaw Resistance (ASTM C666A; 600 cycles)	RDM = 112%
Alkali-Silica Reaction (ASTM C1260; tested for 28 days)	Innocuous

Research published by the Federal Highway Administration in 2006 investigated a number of material properties of UHPC in a material characterization study.[3] The research analyzed both mechanical- and durability-based behaviors of UHPC to validate use in future highway and bridge construction projects. A matrix of curing regimes were selected in order to further evaluate the behaviors, since actual field conditions may vary depending on availability of resources and facilities, ambient environmental conditions, and application of the element constructed of UHPC.

The compressive mechanical response results from (3) were compiled and presented in (4). The present study generated similar types of results in topics including rate of mechanical property development and relationships between compressive mechanical properties.

Other FHWA research on UHPC compressive mechanical response was presented in (5). This research investigated the use of a variety of cylinder and cube geometries for the determination of compressive strength.

Similar to the research completed in (3), another characterization study (6) also investigated strength and durability of UHPC under four curing regimes. The compressive strength of UHPC cured under ambient laboratory conditions was 14.4, 19.9, 22.3, and 23.9 ksi (99.3, 137.2, 153.8, and 164.8 MPa), respectively, when tested at 3, 7, 14, and 28 days. Specimens exposed to 194°F steam treatment reached 30.3 ksi (208.9 MPa) by 7 days and minimally increased to 31.1 ksi (214.4 MPa) at 28 days. These results indicated that steam treatment of UHPC resulted in rapid hydration at early ages, achieving a higher compressive strength at 7 days than air cured specimens at 28 days.

CHAPTER 3. MATERIAL DETAILS, SPECIMEN FABRICATION, AND TESTING

INTRODUCTION

Details regarding the batching, mixing, and casting of the UHPC-RS test specimens are presented in this chapter. The various curing conditions applied and the methods of testing are also described.

MATERIAL AND SPECIMEN DETAILS

The intent of this study was to capture the compressive mechanical properties of Ductal JS1100RS, a rapid-strengthening ultra-high performance concrete (UHPC-RS). This research was focused on assessing these properties at various ages and curing conditions. In this study, all tests were completed through the use of 3 in. (76.2 mm) nominal diameter cylinders with lengths of approximately 6 in. (152.4 mm).

The UHPC-RS used for this research was obtained from the manufacturer, Lafarge North America. This concrete is similar to other products in the same UHPC product line in that the constituents include a blended cementitious premix powder, water, water-reducing admixtures, and steel fiber reinforcement. The rapid strengthening premix blend arrived in prepackaged, 50-lb. (22.7-kg) bags, while the water-reducing admixtures were shipped in 5-gal. (18.9-liter) plastic jugs. Brass-coated steel fibers arrived in a box weighing 44.1 lb (20 kg). When mixed according to the manufacturer's suggested mixture proportions, a single pallet of UHPC-RS and its associated constituents will yield approximately 17 ft^3 (0.63 yd^3) of material.

Two shipments of premix were used in this study. One pallet arrived in June 2011, while the other arrived in August 2011. The steel fibers and superplasticizers each arrived in shipments separate from the premix. The manufacturer describes the premix as a blend of silica fume, ground quartz, sand, and cement. Though the proportions of each are proprietary for this UHPC, approximate quantities of constituents in this product line have been documented in other research studies.[3] These proportions are provided in Table 2.

Table 2. Typical field-cast UHPC mix composition.

Material	Amount (kg/m^3 (lb/yd^3))	Percent by Weight
Portland Cement	712 (1,200)	28.5
Fine Sand	1,020 (1,720)	40.8
Silica Fume	231 (390)	9.3
Ground Quartz	211 (355)	8.4
Superplasticizer	30 (51)	1.2
Steel Fibers	156 (263)	6.2
Water	130 (218)	5.2

The two water-reducing admixtures provided with the UHPC-RS were products of Chryso, Inc. Fluid Optima 100 is a modified phosphonate plasticizer. Fluid Premia 150 is a modified polycarboxylate high-range water-reducing admixture. Optima 100 and Premia 150 were included in batches according to the UHPC-supplier's recommended mix proportions.

The steel fibers supplied with the UHPC were nondeformed, cylindrical, high-tensile strength steel. They have a diameter of 0.008 in. (0.2 mm) with a length of 0.5 in. (12.7 mm). The steel fibers have a thin brass coating which provides lubrication during the drawing process and provides corrosion resistance for the raw fibers. Steel fibers in UHPC are generally proportioned as a percent of total volume, commonly at 2 percent. This volumetric percentage was prescribed by the UHPC supplier. Table 3 provides the mix proportions for the standard UHPC-RS mix, based on a 1-ft^3 (0.028-m^3) design yield.

Table 3. Standard UHPC-RS Mix Proportions

Material	Amount (lb/ft^3 (kg/m^3))	Percent by Weight
Premix	137.029 (2195)	86.7
Water	9.364 (150)	5.9
Premia 150	1.124 (18)	0.7
Optima 100	0.749 (12)	0.5
Steel Fibers	9.739 (156)	6.2

To potentially accelerate the strength gain, the UHPC supplier recommended that Rheocrete CNI, a calcium nitrite-based, corrosion-inhibiting admixture from the BASF Chemical Company, be added to the mix design. An additional mix design utilizing CNI was added to the test plan. The modified mixture proportions are provided in Table 4.

Table 4. Modified UHPC-RS Mix Proportions

Material	Amount (lb/ft^3 (kg/m^3))	Percent by Weight
Premix	137.029 (2195)	86.5
Water	8.578 (137)	5.4
Premia 150	0.936 (15)	0.6
Optima 100	0.936 (15)	0.6
BASF CNI	1.124 (18)	0.7
Steel Fibers	9.739 (156)	6.2

TEST MATRIX

The test matrix included eight different batches of UHPC-RS. These eight batches afforded the opportunity to investigate the association of the compressive mechanical properties with time as influenced by the curing temperature, the age of the premix at casting, and the addition of the chemical accelerator. Since temperature plays a key role in concrete mechanical property development and varies with weather and region, a series of temperatures were selected to test a range of curing conditions. Once cast, specimens would be placed directly into the prescribed curing environment where they remained until one hour before testing. Three curing temperatures were selected: 50°F, 73°F, and 105°F (10°C, 23°C, and 40°C). Specimens subjected to 50°F (10°C) curing were placed in a temperature-controlled environmental chamber. Specimens subjected to 73°F (23°C) curing were allowed to cure in the standard laboratory environment. The specimens subjected to 105°F (40°C) curing were placed inside a walk-in environmental chamber. In all cases, specimens were covered with polyethylene sheeting during the first 24 hours of curing. Table 5 presents the list of batches and their respective curing conditions. Note that the curing temperature for batch SG4 deviated from the intended curing condition. A malfunctioning control unit on the environmental chamber allowed the applied temperature to surpass the programmed value. Also, the testing represented by batch SG7 was repeated in batch SG8 in order to verify the results observed.

Table 5. UHPC-RS Batches and Curing Condition

Batch Name	Mix Design[†]	Blend	Shipment Received	Age at Casting	Curing Temperature
SG1	S	March	June	5 mo.	73°F (23°C)
SG2	S	March	June	5 mo.	50°F (10°C)
SG3	S	June	August	2.5 mo.	105°F (40°C)
SG4	S	March	June	6 mo.	105+°F (40+°C)[‡]
SG5	S	June	August	3 mo.	50°F (10°C)
SG6	S	June	August	3 mo.	73°F (23°C)
SG7	M	June	August	3 mo.	105°F (40°C)
SG8	M	June	August	3.5 mo.	105°F (40°C)

[†] S = Standard, M = Modified

[‡] Temperature ranged from 105°F (40°C) to 118°F (48°C) during the curing process.

As shown in the table, the two different shipments of UHPC-RS allowed the age of the premix at casting to be investigated. Finally, the inclusion of the accelerator to the mix design was investigated in batches SG7 and SG8.

MIXING, CASTING, AND DEMOLDING

Mixing of the material was achieved through the use of a 1930s era pan mixer with a capacity of 2 ft^3 (0.057 m^3). Though not as efficient and powerful as modern pan mixers, this mixer was capable of appropriately mixing the UHPC-RS. Mixing times varied depending on the age of the premix since blending, but were generally around 15 minutes to 20 minutes for the newer and older blends, respectively. Thirty-three cylinders were cast for each batch, allowing compression testing at a variety of ages. The design yield of each batch was 1 ft^3 (0.028 m^3).

The mixing process used for the UHPC-RS differed from that used for conventional concrete due to the nature of the material. As per the UHPC supplier's recommendation, both the Premia and Optima (and CNI, when applicable) were added directly to the mixing water. The premix powder was added to a dry mixing pan and mixing began. Over the course of the first two minutes, the liquids were added slowly and consistently to the premix. When the material could be considered a paste, the steel fibers were slowly added over the course of one minute. Once the fibers appeared to be sufficiently incorporated, which required approximately three minutes, mixing ceased and the molds were filled.

Regarding the casting of the specimens, since the UHPC-RS contained steel fibers, rodding the cylinders as a means of consolidation was not permitted. This was remedied by casting each cylinder in a single-use, plastic mold, then providing external vibration on a portable vibrating table for between 10 and 20 seconds. Specimens were filled in one lift due to the high flowability of the material. The exposed surface on the top of each cylinder was finished using a magnesium hand float. Exposed tops of the cylinders were protected from desiccation by a thin polyethylene sheet, which was applied immediately following the finishing process. This sheet remained in place throughout the first 24 hours, regardless of the curing condition to which the cylinders were exposed.

In order to allow specimens to remain in their respective curing conditions for as long as possible before being tested, cylinders were typically stripped immediately prior to preparation for testing. As such, and especially in cases of tests during the initial 24 hours, specimens cured at 50°F (10°C) or 105°F (40°C) were generally removed 1 hour prior to their scheduled test time. Early-age UHPC-RS cylinders required special care when removing the mold due to the material exhibiting low strength. These cylinders were demolded by continuous vertical scoring of the mold with a utility knife. The mold was then removed by hand to avoid damage. Cylinders cured for a minimum of 24 hours were demolded using a standard cylinder stripping tool, as the UHPC-RS was sufficiently strong to resist any damage imparted by the stripping tool.

END PREPARATION OF CYLINDERS

Before compression and modulus testing began, cylinder ends were prepared by either sulfur mortar capping or cylinder end grinding. Past experience has demonstrated that grinding UHPC cylinders at early ages can result in a damaged end surface with torn-out fibers. Specimens expected to exhibit less than f_c' = 12 ksi (82.7 MPa) were capped with a high-strength sulfur mortar compound suitable for materials with strengths of up to f_c' = 16 ksi (110 MPa). Forney Hi-Cap capping compound was selected for its compressive strength range and low odor/vapor emissions. Capping of cylinders utilized a Humboldt vertical capping stand and capping plate, which is finished to within 0.002-in. (0.05-mm) planeness. Due to the capping system used, parallel and planeness of capped cylinder ends was assumed to meet the requirements of ASTM C39 and C469.

Cylinders expected to exhibit compressive strength greater than f_c' = 12 ksi (82.7 MPa) at time of testing were ground on both ends using a cylinder end grinder with diamond grinding wheel. To ensure that parallel and planeness standards set forth by ASTM were met, each ground cylinder was inspected using a dial indicator. The cylinder was placed on a base plate with the dial indicator directly above and in contact with the top of the cylinder. When rotated, the dial indicator would contact the top surface around the entire perimeter, measuring the shortest and longest lengths to within 0.001-in. (0.0255-mm) accuracy. This method was used to ensure that the ends of each cylinder were parallel to within 0.57 degrees, with the large majority of the cylinders being within 0.5 degrees. On the rare occasions when the limit was exceeded, the cylinder was reground until a satisfactory reading was achieved.

COMPRESSIVE MECHANICAL BEHAVIOR TESTING

The test program was designed to investigate the compressive mechanical response of a rapid-strengthening UHPC. To complete this task, common cylinder compression test methods were engaged. Through these tests, the axial load and axial strain on the cylinder were collected from initial load application through failure of the specimen. As such, the compressive stress-strain response through the attainment of the compressive strength was captured.

All tests were completed on 3 in. (76.2 mm) nominal diameter cylinders with approximately 6 in. (152.4 mm) lengths. The tests were completed through a modified version of the ASTM C39 *Standard Test Method for Compressive Strength of Cylindrical Concrete Specimens* and ASTM C469 *Standard Test Method for Static Modulus of Elasticity and Poisson's Ratio of Concrete in Compression* tests.[7,8] The employed test method has been engaged multiple times in the past to capture the stress-strain response of UHPC.[3,4,12,13]

From the standpoint of the ASTM C39 test method, the two modifications included that the load rate was increased and that the axial strain was captured during the test. The specified loading rate of 35 psi/second (0.24 MPa/second) was changed to 150 psi/second (1.0 MPa/second) due to the high compressive strength of UHPC and the duration of test which would result from the slower load rate.

The axial strain was measured through the use of a parallel ring compressometer. This device is similar to the traditional compressometer described in ASTM C469, except that it holds three LVDTs and does not use a hinge to multiply the deformations. The top ring held the three LVDTs spaced equidistant around the perimeter of the ring and which bore down onto the bottom ring. The gage length between the centers of the two rings was set at 2 in. (50.8 mm). Using this apparatus, the axial deformation of the cylinder was measured and recorded throughout the entire compressive loading of the cylinder.

Data acquisition of the loads and displacements was accomplished with a laptop computer and software designed to connect and communicate with both the compression test machine and the three LVDTs. ASTM C469 specifies the test be completed in a minimum of two separate loadings, with the first set of load data being discarded. Loading should not exceed 40 percent of the peak compressive strength (ultimate load). Testing for this study, however, followed the alternative given in section 6.5 of ASTM C469, which allows for the simultaneous collection of both compressive strength and modulus of elasticity, so long as the LVDTs are either protected from damage at failure or disposable.

The three specific parameters captured during each test included the compressive strength, the modulus of elasticity, and the strain at peak strength. Stresses are defined as the applied load divided by the average cross-sectional area. Strains are defined as the average axial deformation divided by the gage length. The compressive strength and the strain at peak strength were both captured at the peak load applied to each cylinder. The modulus of elasticity was calculated based on a linear best-fit approximation of the slope of the stress-strain response between 10 percent and 30 percent of the peak stress applied to a specimen. Given that the stress and strain data were collected through the entire test, post-processing of the data allowed the modulus of elasticity to be calculated over this precise stress range.

Prior to the start of testing, each cylinder was measured for diameter and length. Two diameters were recorded at approximately the third-points of the length of the cylinder and three lengths at third points around the circumference. Cylinder lengths of sulfur capped specimens included the thickness of the sulfur caps in the measurement.

All cylinders were tested in a Forney compression testing machine having a 1,000-kip (4.45-kN) capacity. This hydraulic actuated testing machine uses a needle value to set an oil flow rate. As such, the flow rate was set early in each test so that the appropriate load rate was achieved during the stiffest portion of the response. The oil flow rate was not modified as the specimen neared failure.

CHAPTER 4. TEST RESULTS

INTRODUCTION

The test results from the physical testing of the UHPC-RS cylinders are presented in this chapter. Specific results pertaining to compressive strength, strain at compressive strength, and modulus of elasticity are presented. Additionally, compressive stress-strain response results are presented.

TEST RESULTS

The results from each of the approximately 33 tests in each of the 8 batches were collected and analyzed to determine the compressive mechanical behaviors. Figure 1 illustrates the results obtained from one cylinder in batch SG1. Similar results for all cylinders tested in this research were compiled. All batches were tested through 56 days. Note that errors related to specimen preparation, test setup, or data acquisition occurred on a small number of specimens. Any inappropriate data collected from these specimens was not included in the analysis and has been discarded from use in this report.

SG1-23

Average Diameter =	77.0 mm	(3.030 in.)
Average Length =	150.9 mm	(5.941 in.)
Area =	4652.0 mm^2	(7.211 sq.in.)
Maximum Stress =	127.3 MPa	(18.47 ksi)
Modulus of Elasticity Gage Length =	50.8 mm	(2.000 in.)
MoE: 10% of Maximum Stress =	12.7 MPa	(1.85 ksi)
MoE: 30% of Maximum Stress =	38.2 MPa	(5.54 ksi)
Modulus of Elasticity =	45.5 GPa	(6590 ksi)
Strain at Maximum Stress =	0.003928	

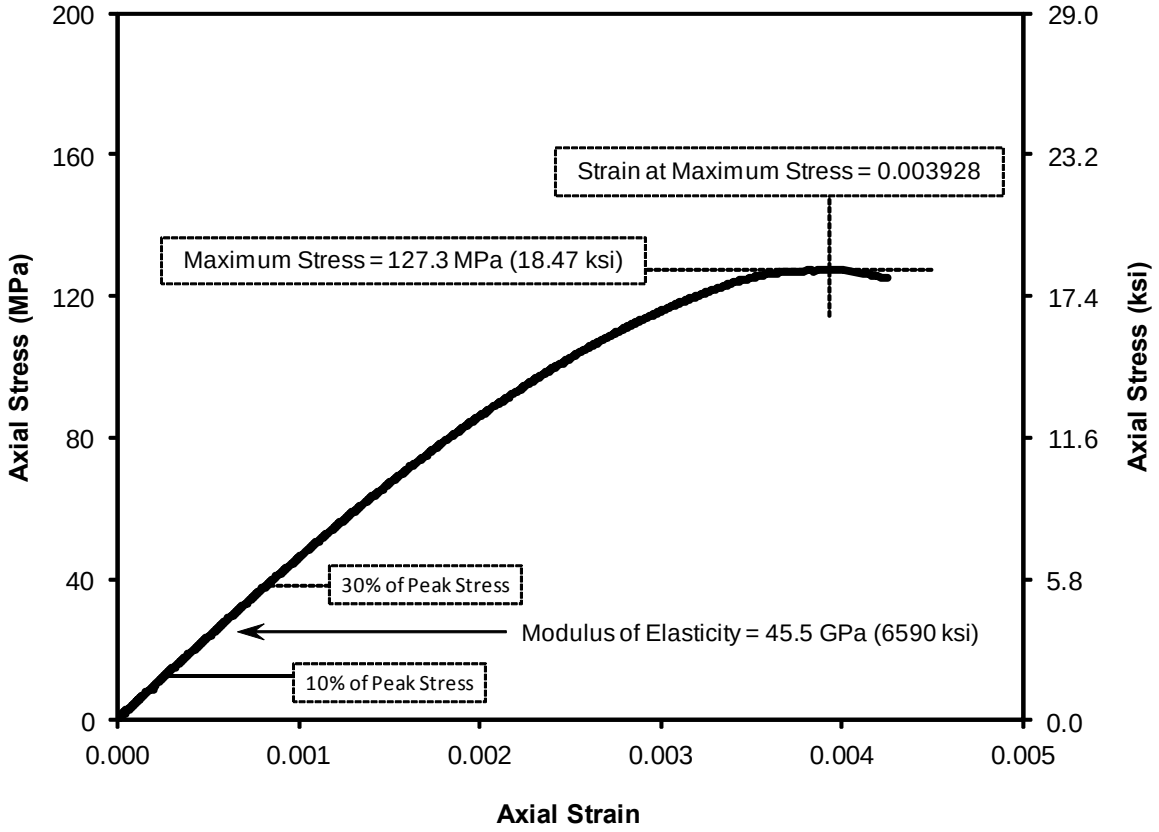

Figure 1. Graph. Specimen SG1-23 compressive mechanical response.

For each batch of specimens, tables containing the test results were constructed. These are presented beginning with Table 6 and ending with Table 13. Each table displays the most relevant test information, including the age of the cylinders at the time of testing, end preparation method (SC = sulfur capped, G = ground), specimen length-to-diameter ratio, peak stress, modulus of elasticity, and strain at peak stress. To summarize for a particular testing age, there are additional columns that present the average values for peak stress, modulus of elasticity, and strain at peak stress. Additionally, results from a specimen for which a particular parameter was not captured are displayed as "-".

Table 6. Test results for batch SG1.

Age [days]	End Prep	L/D Ratio	f_c' [ksi]	f_c' Avg [ksi]	E_c [ksi]	E_c Avg [ksi]	Strain @ f_c'	Strain @ f_c' Avg
	SC	-	0.43		180		0.017570	
0.36	SC	2.07	0.42	0.45	310	220	0.011260	0.016860
	SC	2.07	0.52		180		0.021750	
	SC	2.11	0.75		380		0.014600	
0.44	SC	2.09	0.79	0.85	300	330	0.013650	0.015680
	SC	2.09	1.01		320		0.018790	
	SC	2.08	1.28		720		0.010670	
0.51	SC	2.08	1.71	1.62	750	770	0.011900	0.012120
	SC	2.11	1.88		850		0.013790	
	SC	2.08	13.17		5790		0.004460	
1.00	SC	2.06	12.98	13.00	5560	5680	0.004620	0.004290
	SC	2.06	12.85		5690		0.003790	
	G	1.95	16.07		6310		0.004130	
1.47	G	1.95	15.39	15.52	6160	6240	0.003980	0.004050
	G	1.97	15.08		-		-	
	G	1.96	16.13		6240		0.004240	
2.00	G	1.97	16.87	16.30	6780	6750	0.004110	0.003810
	G	1.94	15.90		7230		0.003080	
	G	1.95	16.40		6280		0.003790	
3.00	G	1.97	16.79	17.01	6370	6570	0.003750	0.003740
	G	1.95	17.84		7050		0.003670	
	G	1.97	18.40		6840		0.003510	
7.00	G	1.96	18.47	18.48	6590	6720	0.003930	0.003720
	G	1.96	18.57		-		-	
	G	1.96	20.90		-		-	
15.00	G	1.96	21.00	21.41	7140	6920	0.003470	0.003720
	G	1.97	22.33		6690		0.003965	
	G	1.97	23.10		7260		0.003910	
28.00	G	1.96	21.69	22.76	7210	7280	0.003380	0.003670
	G	1.98	23.49		7360		0.003710	
	G	1.94	24.60		7550		0.003670	
56.28	G	1.94	23.29	23.46	7070	7230	0.003940	0.003740
	G	1.92	22.49		7060		0.003620	

1 ksi = 6.895 MPa

Table 7. Test results for batch SG2.

Age [days]	End Prep	L/D Ratio	f_c' [ksi]	f_c' Avg [ksi]	E_c [ksi]	E_c Avg [ksi]	Strain @ f_c'	Strain @ f_c' Avg
	SC	2.08	0.44		40		0.013000	
0.61	SC	2.07	0.44	0.47	60	70	0.014340	0.014530
	SC	2.08	0.54		120		0.016250	
	SC	2.09	0.80		240		0.011590	
0.70	SC	2.08	0.76	0.82	210	240	0.016320	0.015590
	SC	2.08	0.89		260		0.018860	
	SC	2.08	1.03		520		0.011750	
0.79	SC	2.08	1.30	1.11	480	460	0.013980	0.012300
	SC	2.07	1.01		380		0.011180	
	SC	2.10	1.45		830		0.011380	
0.87	SC	2.07	1.62	1.64	960	1010	0.012810	0.011050
	SC	2.07	1.84		1230		0.008970	
	SC	2.09	2.21		1790		0.008750	
0.95	SC	2.11	2.19	2.38	1610	1650	0.008220	0.009610
	SC	2.10	2.74		1550		0.011850	
	G	1.95	11.88		5400		0.005910	
1.84	G	1.97	11.70	11.92	3620	5200	0.005960	0.005620
	G	1.95	12.18		6570		0.004990	
	G	1.94	17.08		6510		0.004480	
8.00	G	1.94	16.09	16.68	-	6530	-	0.004200
	G	1.94	16.88		6550		0.003910	
	G	1.95	18.86		6630		0.004440	
14.00	G	1.95	18.46	18.66	6910	6750	0.004130	0.004260
	G	1.96	18.66		6710		0.004210	
	G	1.95	20.42		6770		0.004250	
28.00	G	1.95	20.11	20.12	6980	6740	0.004110	0.004230
	G	1.96	19.84		6480		0.004320	
	G	1.91	21.72		6850		0.004040	
55.72	G	1.91	21.86	21.67	7620	7250	0.003650	0.003750
	G	1.91	21.43		7290		0.003550	

1 ksi = 6.895 MPa

Table 8. Test results for batch SG3.

Age [days]	End Prep	L/D Ratio	f_c' [ksi]	f_c' Avg [ksi]	E_c [ksi]	E_c Avg [ksi]	Strain @ f_c'	Strain @ f_c' Avg
	SC	2.08	0.43		50		0.025160	
0.16	SC	2.08	0.45	0.43	40	60	0.035700	0.031010
	SC	2.09	0.42		80		0.032170	
	SC	2.07	0.60		140		0.023180	
0.27	SC	2.09	0.82	0.75	90	130	0.037870	0.028810
	SC	2.09	0.82		170		0.025370	
	SC	2.07	2.70		830		0.034840	
0.36	SC	2.07	2.40	2.80	1330	1170	0.006100	0.021160
	SC	2.08	3.29		1360		0.022530	
	SC	2.08	7.96		4260		0.006630	
0.42	SC	2.07	8.41	8.42	4690	4510	0.004980	0.005530
	SC	2.08	8.90		4570		0.004980	
	SC	2.06	12.89		5620		0.004280	
0.50	SC	2.09	12.72	12.91	5690	5630	0.003680	0.004000
	SC	2.08	13.13		5580		0.004030	
	G	1.95	19.00		6460		0.003750	
1.00	G	1.96	18.04	18.36	7140	6780	0.003020	0.003360
	G	1.96	18.02		6750		0.003310	
	G	1.96	19.08		7110		0.003470	
2.00	G	1.96	20.80	19.93	-	7110	-	0.003470
	G	1.95	19.92		-		-	
	G	1.94	19.81		7050		0.003340	
7.00	G	1.97	22.38	21.61	6760	7070	0.003930	0.003540
	G	1.97	22.63		7410		0.003360	
	G	1.97	23.55		7330		0.003560	
14.00	G	1.96	22.79	23.37	7620	7390	0.003090	0.003440
	G	1.96	23.76		7230		0.003660	
	G	1.94	24.30		7800		0.003590	
28.06	G	1.95	24.55	23.87	7380	7550	0.003690	0.003490
	G	1.97	22.75		7480		0.003200	
	G	1.91	24.57		7300		0.003890	
56.05	G	1.94	-	26.01	-	7440	-	0.003920
	G	1.96	27.45		7570		0.003960	

1 ksi = 6.895 MPa

Table 9. Test results for batch SG4.

Age [days]	End Prep	L/D Ratio	f_c' [ksi]	f_c' Avg [ksi]	E_c [ksi]	E_c Avg [ksi]	Strain @ f_c'	Strain @ f_c' Avg
	SC	2.05	0.45		140		0.024850	
0.21	SC	2.06	0.44	0.46	130	160	0.018330	0.021170
	SC	2.04	0.48		220		0.020340	
	SC	2.06	1.17		300		0.019660	
0.32	SC	2.05	1.37	1.36	-	440	-	0.017190
	SC	2.06	1.55		580		0.014720	
	SC	2.05	5.37		3660		0.011290	
0.39	SC	2.05	5.97	5.96	3960	3880	0.004900	0.007510
	SC	2.05	6.55		4020		0.006350	
	SC	2.07	9.04		4990		0.003440	
0.44	SC	2.08	8.50	9.36	5060	5110	0.002870	0.003460
	SC	2.07	10.56		5280		0.004070	
	SC	2.07	12.81		5890		0.003270	
0.52	SC	2.07	12.54	12.79	5290	5660	0.003740	0.003510
	SC	2.06	13.03		5790		0.003520	
	G	1.89	17.56		6930		0.003020	
1.00	G	1.93	17.50	17.57	6930	6860	0.002940	0.003010
	G	1.95	17.64		6710		0.003080	
	G	1.93	20.89		7320		0.003520	
2.00	G	1.93	18.33	19.81	-	7270	-	0.003300
	G	1.94	20.21		7210		0.003070	
	G	1.95	21.49		7110		0.003320	
7.00	G	1.96	21.03	20.87	7410	7320	0.003240	0.003170
	G	1.93	20.10		7430		0.002950	
	G	1.95	23.46		7590		0.003430	
14.00	G	1.94	22.77	23.62	7230	7440	0.003370	0.003550
	G	1.95	24.63		7500		0.003860	
	G	1.92	18.87		6970		0.002970	
29.17	G	1.95	21.03	19.50	7580	7200	0.003200	0.003020
	G	1.94	18.61		7050		0.002890	
	G	1.89	23.33		6930		0.003870	
56.22	G	1.91	24.67	24.27	7260	7190	0.003890	0.003830
	G	1.91	24.80		7390		0.003730	

1 ksi = 6.895 MPa

Table 10. Test results for batch SG5.

Age [days]	End Prep	L/D Ratio	f_c' [ksi]	f_c' Avg [ksi]	E_c [ksi]	E_c Avg [ksi]	Strain @ f_c'	Strain @ f_c' Avg
	SC	2.02	0.65		200		0.013730	
0.73	SC	2.03	0.71	0.71	370	350	0.011370	0.012040
	SC	2.01	0.77		490		0.011030	
	SC	2.06	1.38		1090		0.010700	
0.85	SC	2.07	1.59	1.55	1310	1310	0.010650	0.009150
	SC	2.04	1.68		1520		0.006110	
	SC	2.04	2.47		1730		0.007740	
0.95	SC	2.03	2.32	2.34	2570	2260	0.003220	0.004340
	SC	2.04	2.22		2470		0.002060	
	SC	2.05	2.40		2830		0.001620	
1.00	SC	2.05	3.07	2.85	3130	3120	0.003100	0.002920
	SC	2.04	3.07		3410		0.004030	
	SC	2.09	7.90		5820		0.002140	
2.00	SC	2.08	6.26	6.96	5940	5880	0.001230	0.001690
	SC	2.04	6.72		-		-	
	G	1.87	16.61		5770		0.004550	
7.00	G	1.91	15.38	16.35	6360	6300	0.003580	0.004180
	G	1.90	17.07		6780		0.004420	
	G	1.87	17.79		-		-	
14.00	G	1.91	18.76	18.22	7030	6800	0.003980	0.004060
	G	1.88	18.13		6570		0.004140	
	G	1.91	22.01		6990		0.004280	
29.00	G	1.88	19.70	21.12	7070	6980	0.003460	0.004110
	G	1.90	21.66		6870		0.004600	
	G	1.88	24.10		-		-	
55.92	G	1.87	23.15	23.50	-	-	-	-
	G	1.85	23.25		-		-	

1 ksi = 6.895 MPa

Table 11. Test results for batch SG6.

Age [days]	End Prep	L/D Ratio	f_c' [ksi]	f_c' Avg [ksi]	E_c [ksi]	E_c Avg [ksi]	Strain @ f_c'	Strain @ f_c' Avg
	SC	2.04	8.90		4800		0.004040	
0.67	SC	2.05	8.86	9.07	5110	5100	0.003950	0.003840
	SC	2.05	9.45		5400		0.003520	
	SC	2.06	11.28		5870		0.003220	
0.80	SC	2.06	10.76	10.94	6040	5860	0.002760	0.003050
	SC	2.05	10.77		5670		0.003180	
	SC	2.05	10.75		5710		0.003050	
0.87	SC	2.05	10.83	11.05	5640	5830	0.003050	0.002980
	SC	2.06	11.58		6140		0.002830	
	SC	2.05	11.68		6060		0.002780	
0.94	SC	2.07	12.54	11.89	6290	6110	0.002920	0.002840
	SC	2.05	11.44		5980		0.002810	
	SC	2.07	11.87		5870		0.002950	
1.00	SC	2.07	12.18	12.14	6340	6150	0.002770	0.002890
	SC	2.07	12.39		6230		0.002960	
	G	1.91	15.67		6130		0.004110	
2.00	G	1.93	15.89	15.92	6470	6300	0.003960	0.004090
	G	1.96	16.22		6300		0.004190	
	G	1.94	20.35		7100		0.003590	
7.00	G	1.94	19.35	19.96	6830	6890	0.003660	0.003700
	G	1.94	20.19		6750		0.003840	
	G	1.93	21.90		7160		0.003440	
14.00	G	1.94	22.06	21.70	7160	7060	0.003790	0.003620
	G	1.94	21.13		6850		0.003630	
	G	1.92	23.10		7330		0.003640	
27.76	G	1.94	23.41	22.58	7330	7120	0.003730	0.003670
	G	1.94	21.24		6710		0.003640	
	G	1.94	24.83		7080		0.003960	
55.91	G	1.92	24.93	25.09	7850	7520	0.003570	0.003780
	G	1.92	25.52		7630		0.003820	

1 ksi = 6.895 MPa

Table 12. Test results for batch SG7.

Age [days]	End Prep	L/D Ratio	f_c' [ksi]	f_c' Avg [ksi]	E_c [ksi]	E_c Avg [ksi]	Strain @ f_c'	Strain @ f_c' Avg
	SC	2.07	0.72		290		0.007920	
0.25	SC	2.05	0.86	0.79	670	580	0.008790	0.007360
	SC	2.04	0.79		780		0.005360	
	SC	2.05	3.75		-		-	
0.36	SC	2.05	3.47	4.14	-	-	-	-
	SC	2.04	5.21		-		-	
	SC	2.05	7.29		5910		0.003320	
0.44	SC	2.06	9.66	8.13	6150	6110	0.002100	0.002250
	SC	2.05	7.43		6260		0.001340	
	SC	2.03	8.73		6370		0.002050	
0.52	SC	2.04	6.77	7.48	6090	6390	0.001740	0.001830
	SC	2.06	6.94		6720		0.001710	
	SC	2.05	9.48		7180		0.001400	
1.00	SC	2.06	9.32	10.22	-	7010	-	0.001670
	SC	2.04	11.86		6840		0.001940	
	G	2.04	10.30		-		-	
1.37	G	2.06	8.95	9.80	-	7200	-	0.001450
	G	2.06	10.14		7200		0.001450	
	G	1.92	19.47		7680		0.003110	
2.00	G	1.90	21.72	20.91	7400	7600	0.003260	0.003210
	G	1.91	21.54		7720		0.003260	
	G	1.91	23.27		7370		0.003700	
7.00	G	1.89	25.41	24.84	7520	7510	0.003810	0.003770
	G	1.92	25.84		7640		0.003790	
	G	1.92	25.63		7750		0.003680	
14.03	G	1.91	25.45	25.62	7680	7810	0.003640	0.003610
	G	1.91	25.78		8010		0.003520	
	G	1.90	26.68		-		-	
28.19	G	1.91	26.99	26.15	-	-	-	-
	G	1.91	24.79		-		-	
	G	1.93	26.49		7890		0.003630	
56.20	G	1.89	26.06	26.23	7880	7770	0.003470	0.003610
	G	1.91	26.15		7540		0.003720	

1 ksi = 6.895 MPa

Table 13. Test results for batch SG8.

Age [days]	End Prep	L/D Ratio	f_c' [ksi]	f_c' Avg [ksi]	E_c [ksi]	E_c Avg [ksi]	Strain @ f_c'	Strain @ f_c' Avg
0.27	SC	2.05	0.95	0.97	540	620	0.009960	0.009300
	SC	2.06	0.92		650		0.009820	
	SC	2.07	1.05		670		0.008130	
0.36	SC	2.07	5.68	5.27	5030	5270	0.001360	0.001350
	SC	2.06	4.78		5490		0.001490	
	SC	2.08	5.35		5290		0.001200	
0.43	SC	2.07	7.26	6.78	7030	6430	0.001390	0.001530
	SC	2.07	5.96		5830		0.001660	
	SC	2.06	7.12		-		-	
1.02	SC	2.07	6.99	8.16	6850	7090	0.001550	0.001890
	SC	2.07	8.93		7230		0.002260	
	SC	2.06	8.56		7200		0.001850	
1.45	SC	2.06	12.51	10.05	7250	7250	0.001900	0.002100
	SC	2.05	9.89		7250		0.002290	
	SC	2.07	7.75		-		-	
2.03	G	2.04	8.76	8.53	-	-	-	-
	G	2.06	8.07		-		-	
	G	2.05	8.76		-		-	
8.16	G	1.92	26.34	24.42	7450	7610	0.003960	0.003570
	G	1.93	25.78		7590		0.003750	
	G	1.91	21.14		7780		0.003010	
14.29	G	1.87	26.22	25.79	5690	6980	0.005270	0.004240
	G	1.92	24.88		7440		0.003780	
	G	1.93	26.26		7800		0.003680	
28.11	G	1.89	27.23	26.67	7140	7330	0.004270	0.004030
	G	1.91	26.21		7220		0.003970	
	G	1.90	26.59		7620		0.003850	
56.23	G	1.90	27.02	26.98	7340	7130	0.004110	0.003950
	G	1.88	21.48*		7270		0.003200	
	G	1.90	27.75		7850		0.003950	
	G	1.88	26.15		6060		0.004530	

* Possible outlier; additional specimen tested at 58d. Avg f_c' does not include this result.
1 ksi = 6.895 MPa

COMPRESSIVE STRENGTH

The compressive strength results for each batch of specimens are presented in Figure 2 through Figure 9. These results, with the average value at each test age also plotted and connected via a dotted line, show the strength gain exhibited by each batch of specimens.

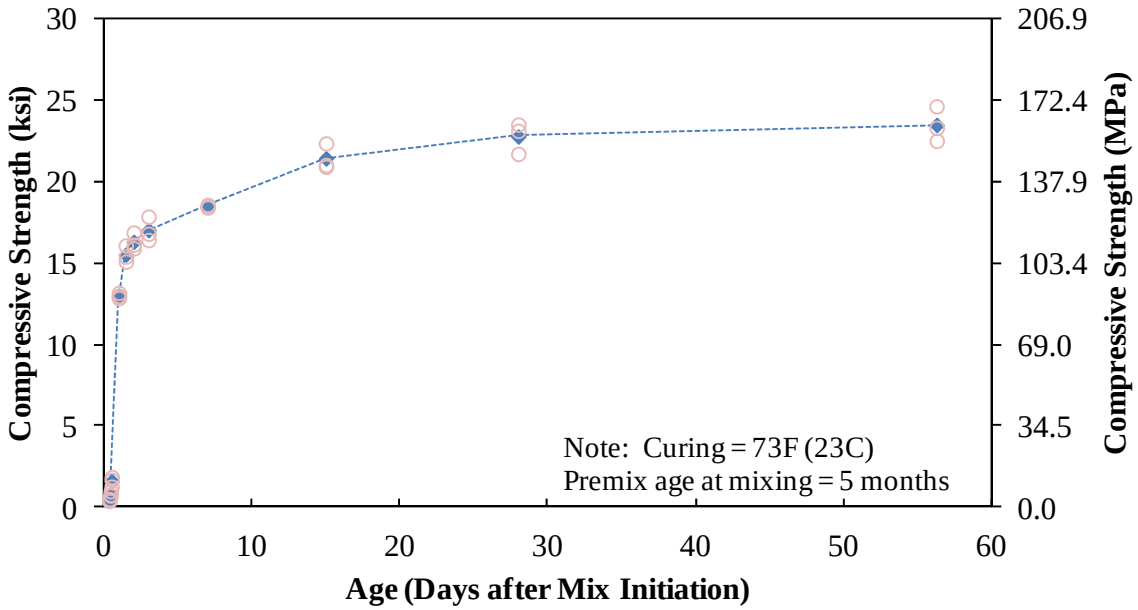

Figure 2. Graph. Strength curve for batch SG1.

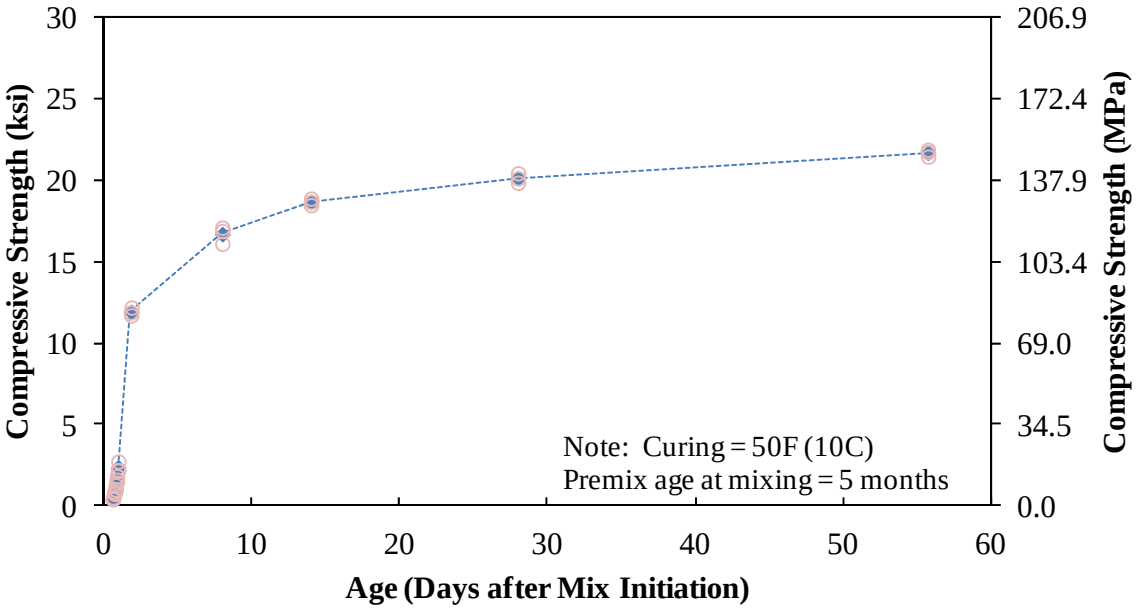

Figure 3. Graph. Strength curve for batch SG2

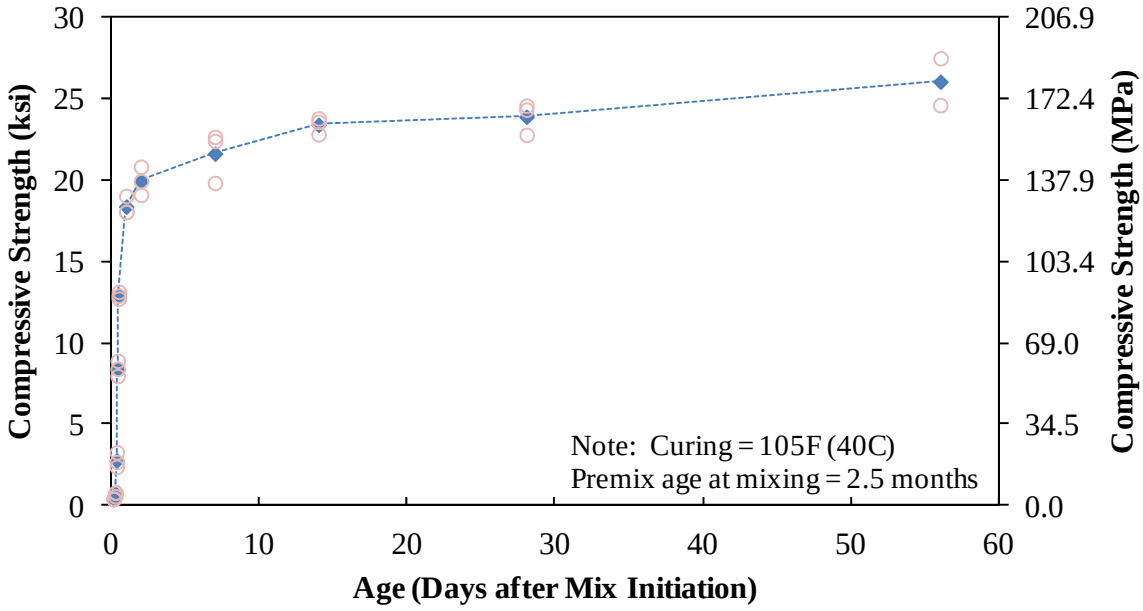

Figure 4. Graph. Strength curve for batch SG3.

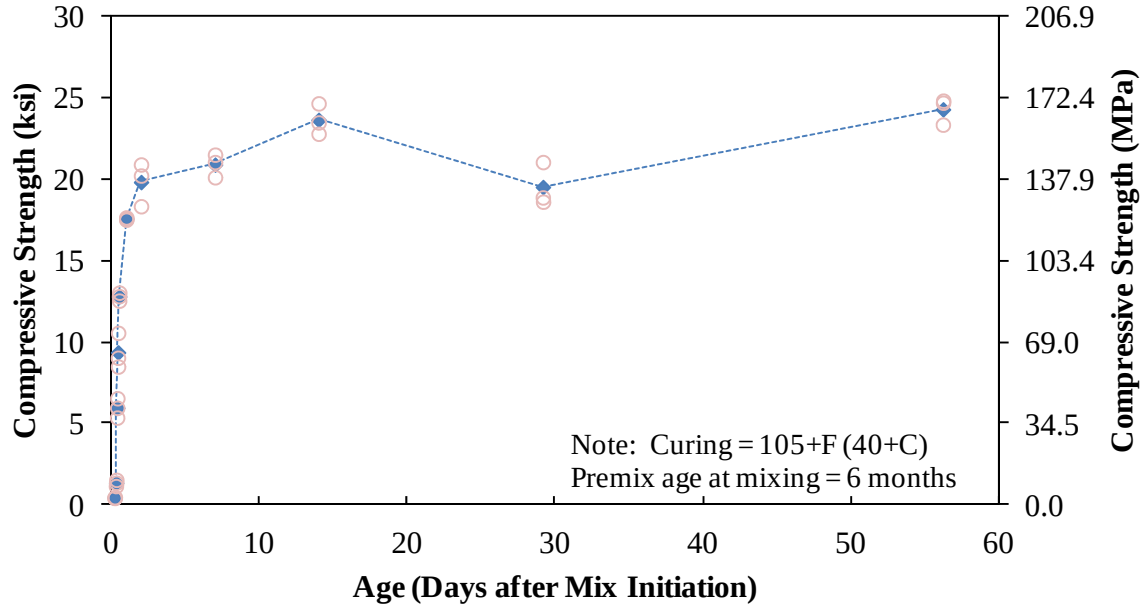

Figure 5. Graph. Strength curve for batch SG4.

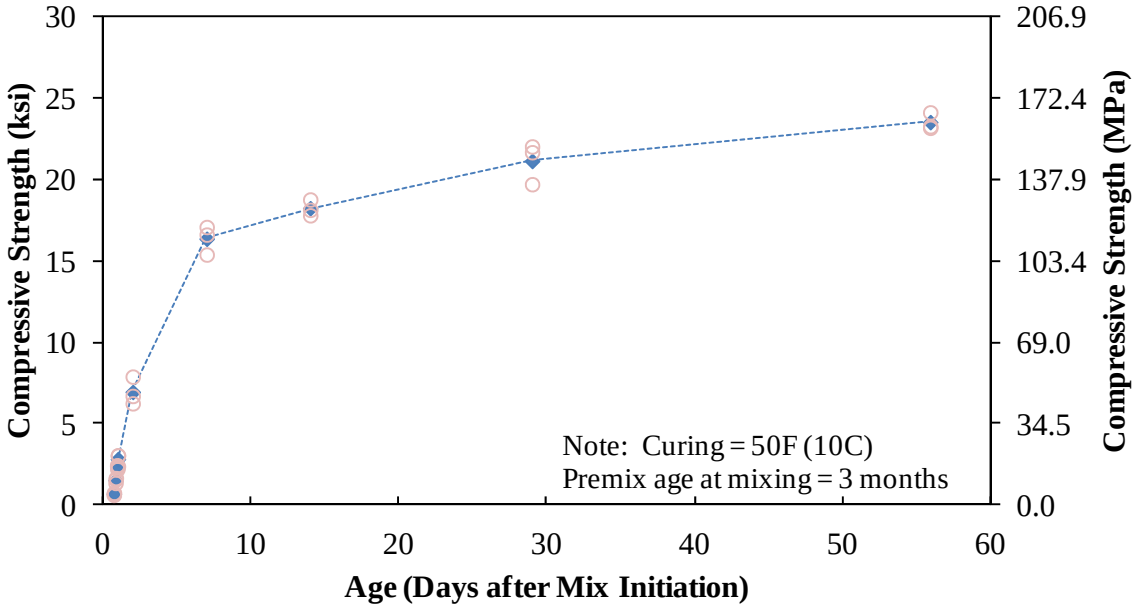

Figure 6. Graph. Strength curve for batch SG5.

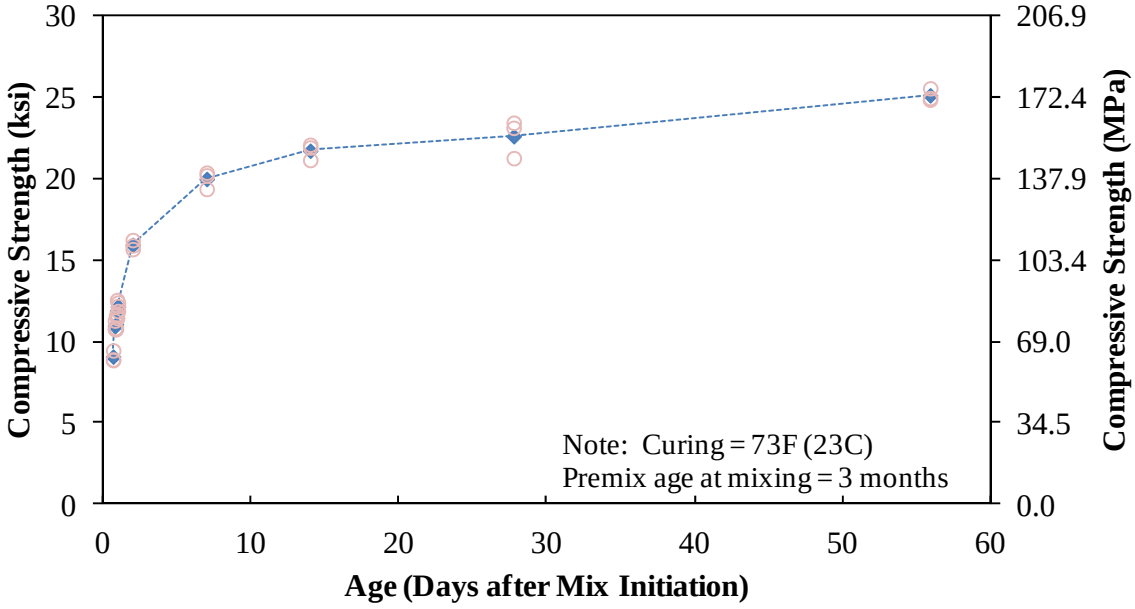

Figure 7. Graph. Strength curve for batch SG6.

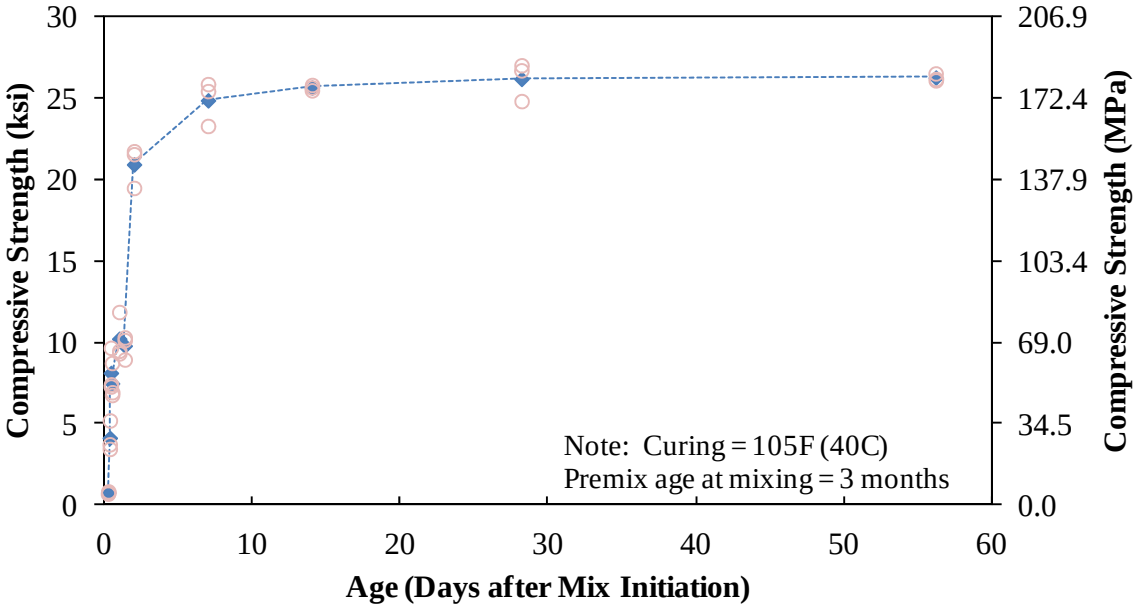

Figure 8. Graph. Strength curve for batch SG7.

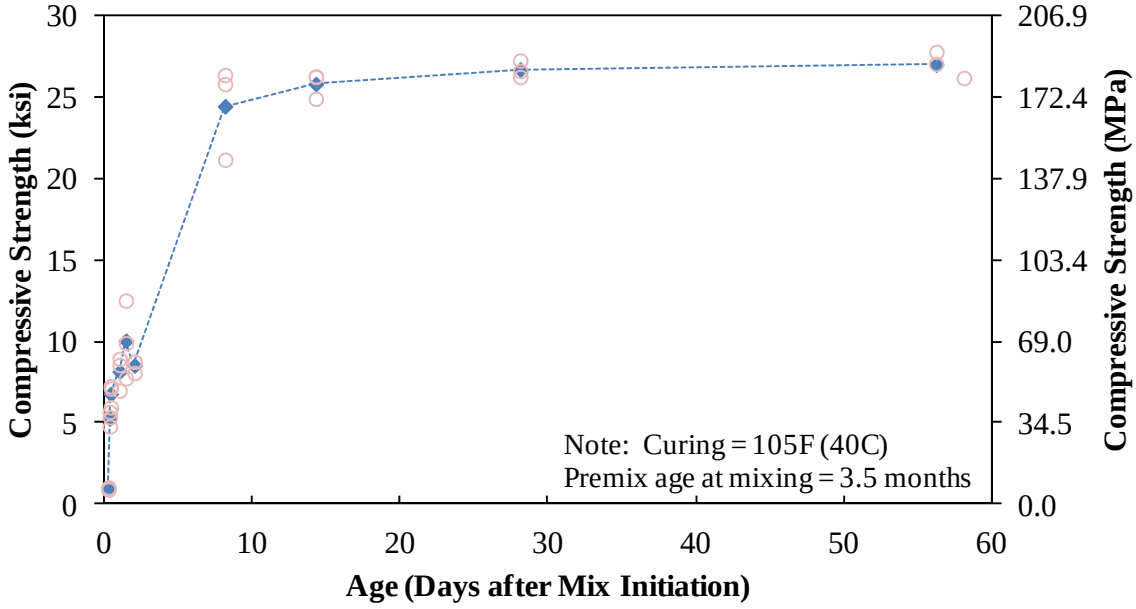

Figure 9. Graph. Strength curve for batch SG8.

MODULUS OF ELASTICITY

The modulus of elasticity results for each batch of specimens are presented in Figure 10 through Figure 17. These results, with the average value at each test age also plotted and connected via a dotted line, show the stiffness gain exhibited by each batch of specimens.

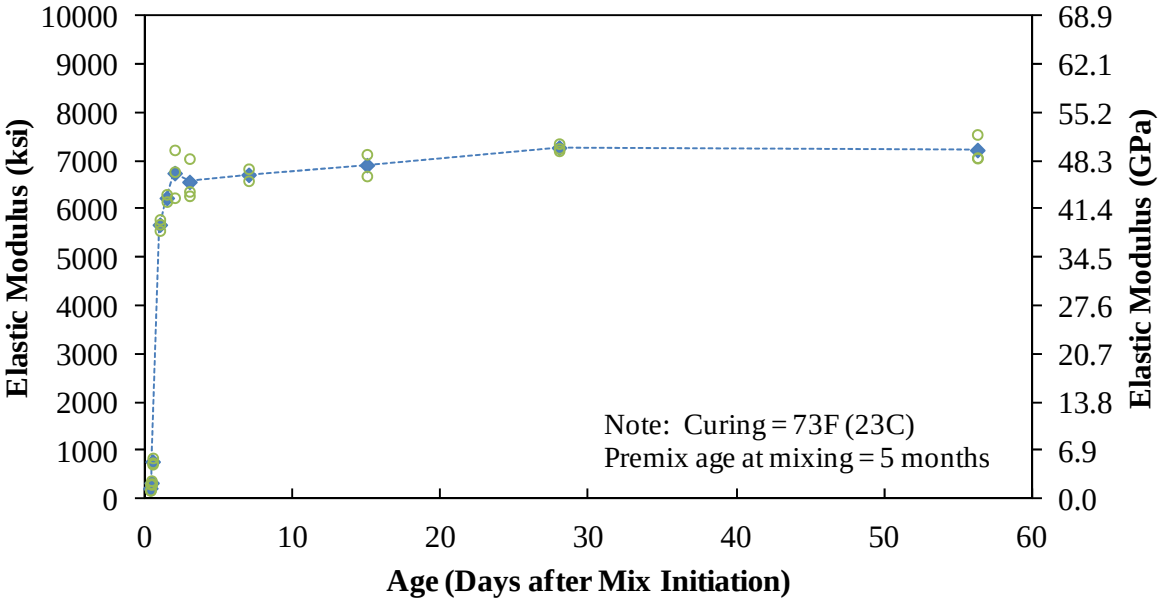

Figure 10. Graph. Elastic modulus curve for batch SG1.

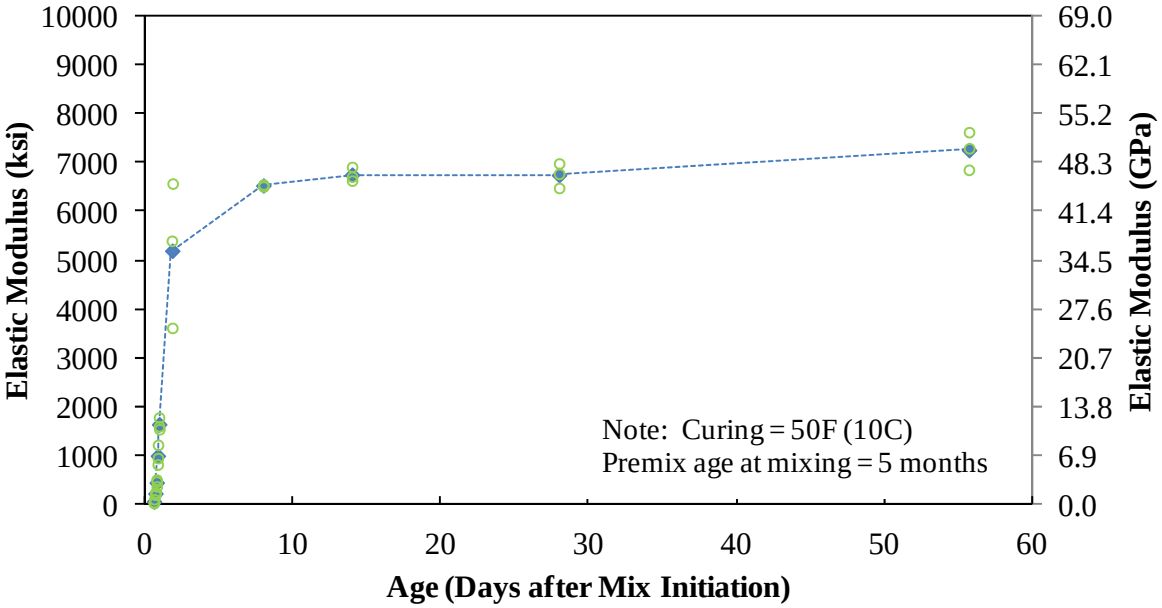

Figure 11. Graph. Elastic modulus curve for batch SG2.

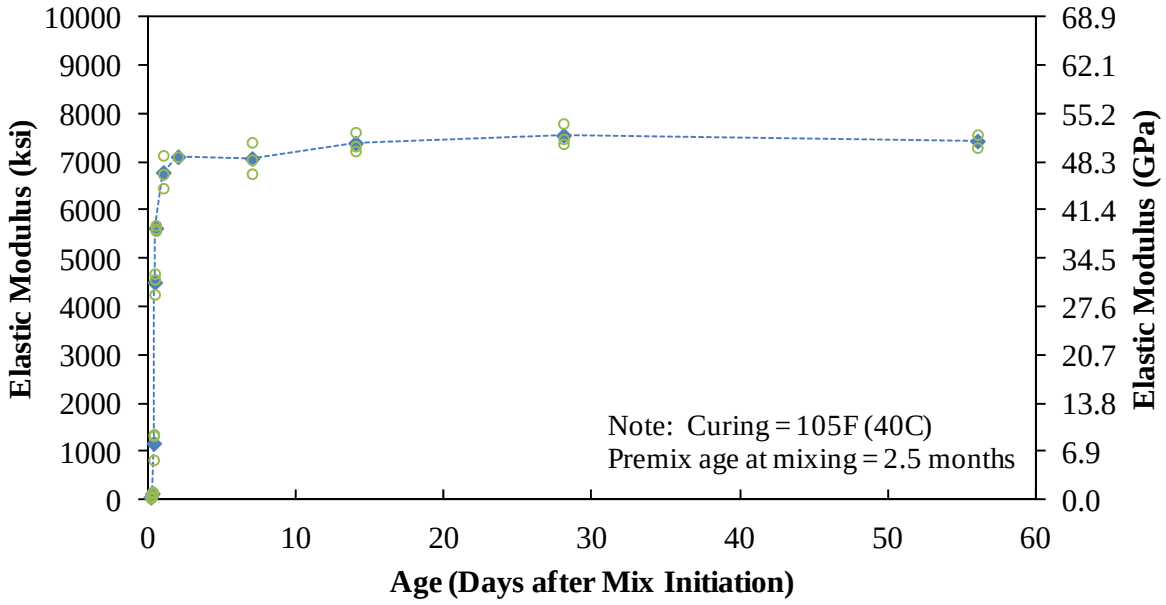

Figure 12. Graph. Elastic modulus curve for batch SG3.

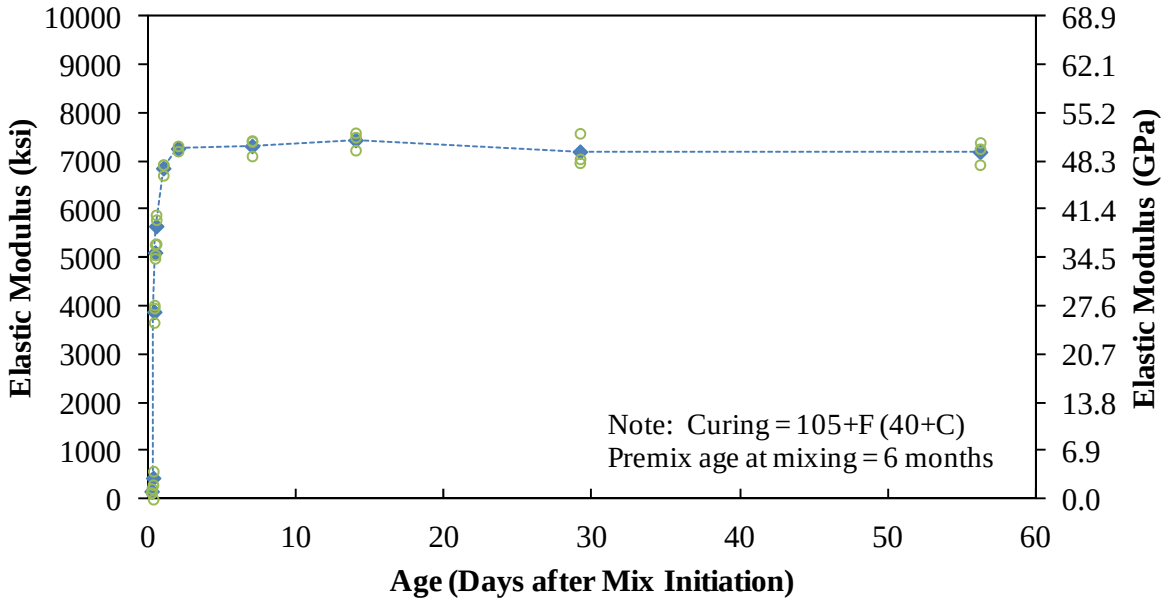

Figure 13. Graph. Elastic modulus curve for batch SG4.

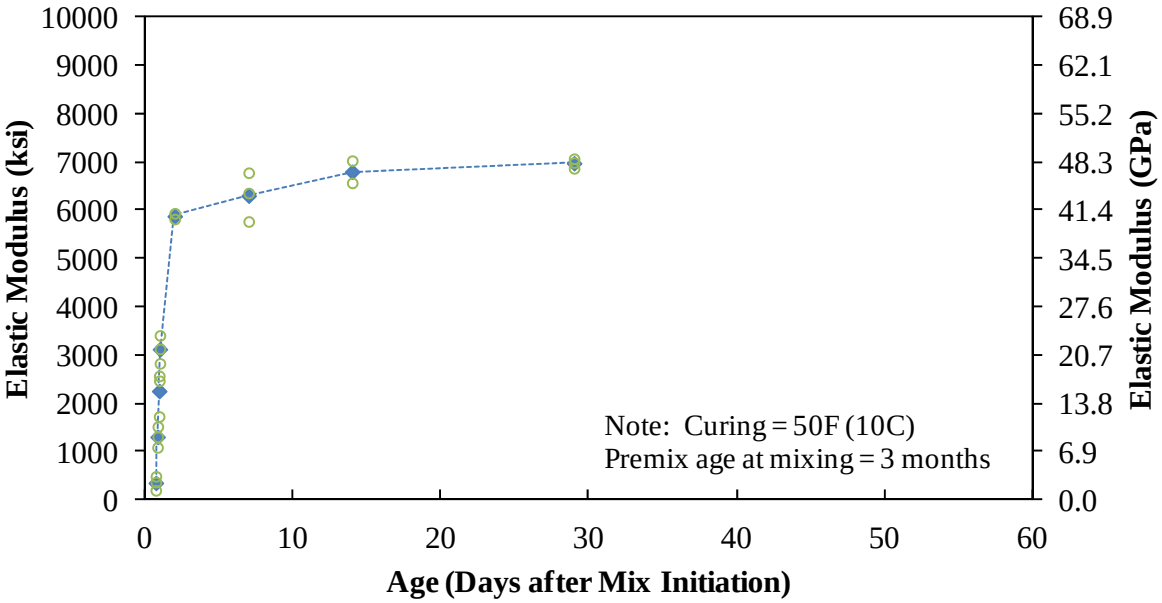

Figure 14. Graph. Elastic modulus curve for batch SG5.

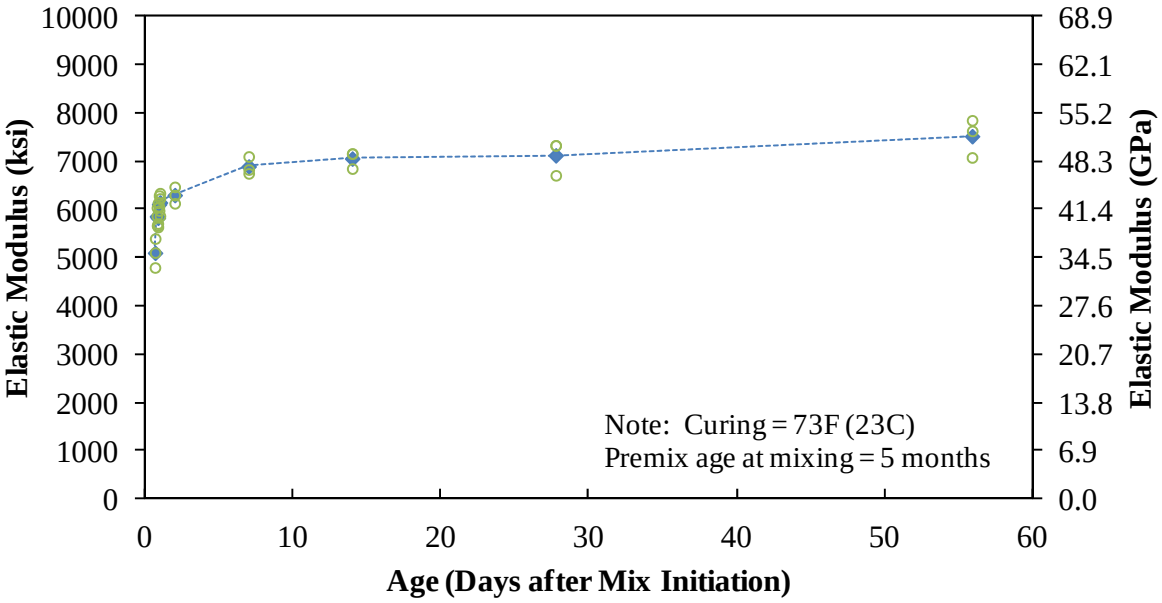

Figure 15. Graph. Elastic modulus curve for batch SG6.

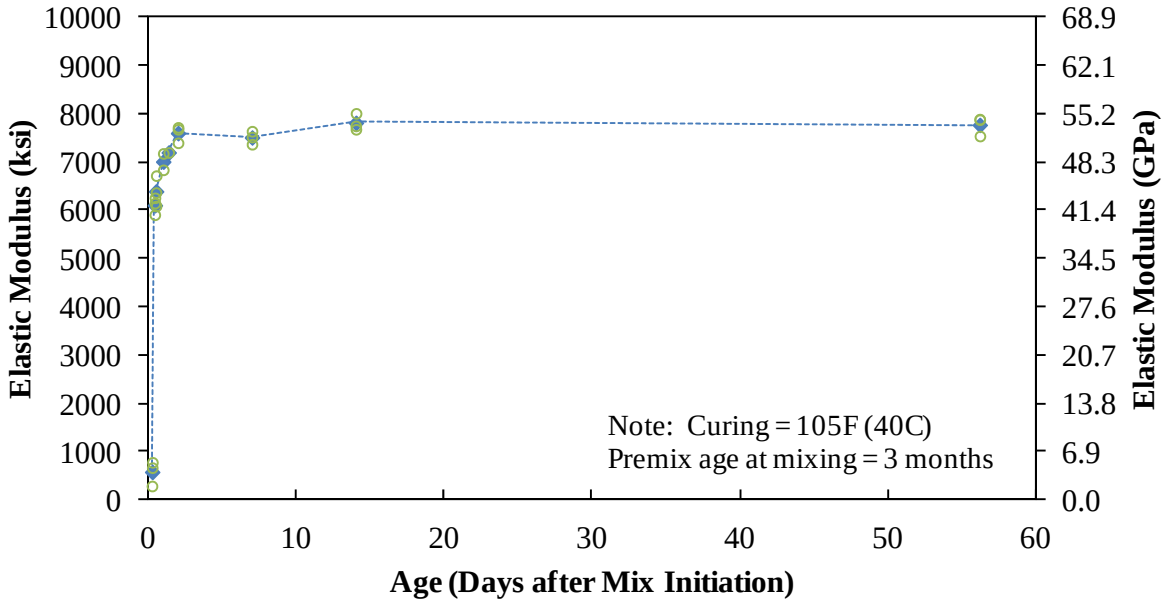

Figure 16. Graph. Elastic modulus curve for batch SG7.

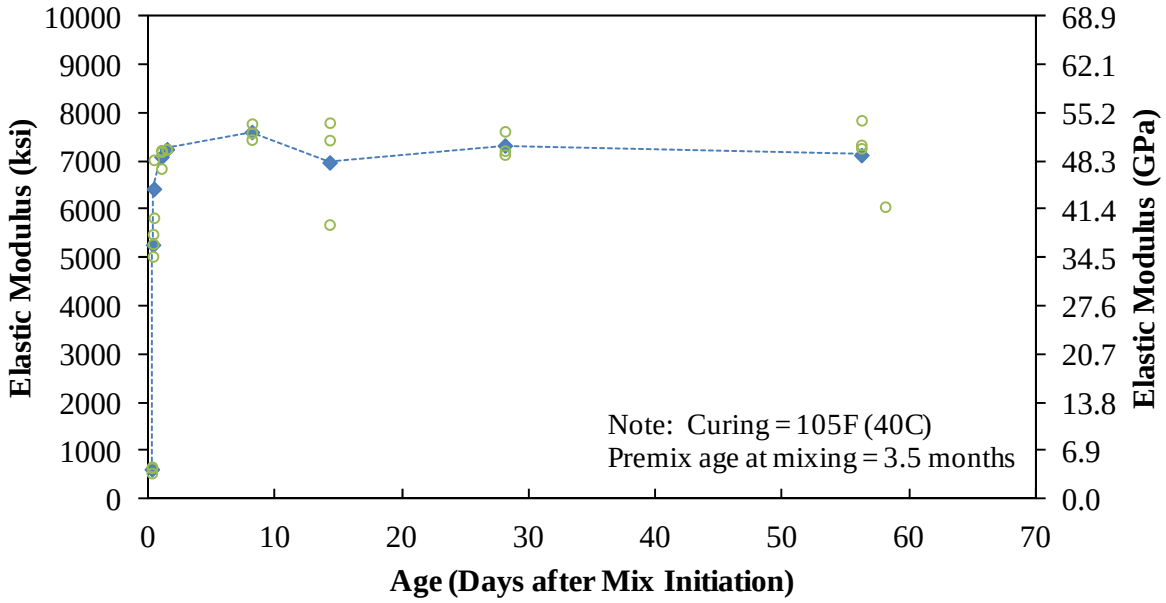

Figure 17. Graph. Elastic modulus curve for batch SG8.

STRAIN AT PEAK STRESS

The strain at peak stress results for each batch of specimens are presented in Figure 18 through Figure 25. These results, with the average value at each test age also plotted and connected via a dotted line, show the strain capacity exhibited by each batch of specimens.

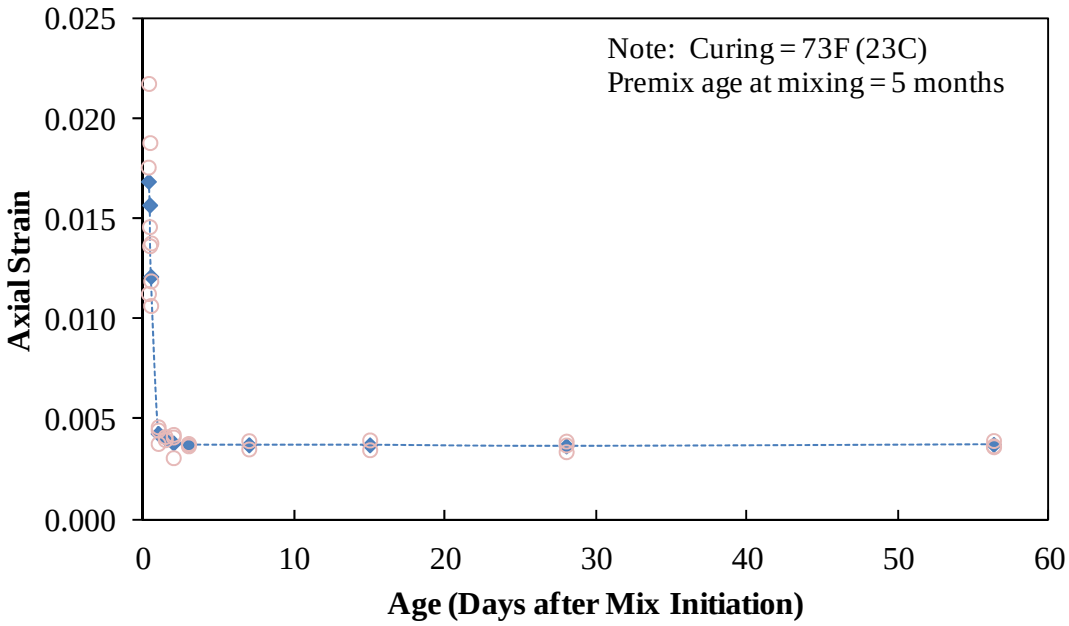

Figure 18. Graph. Strain at peak stress curve for batch SG1.

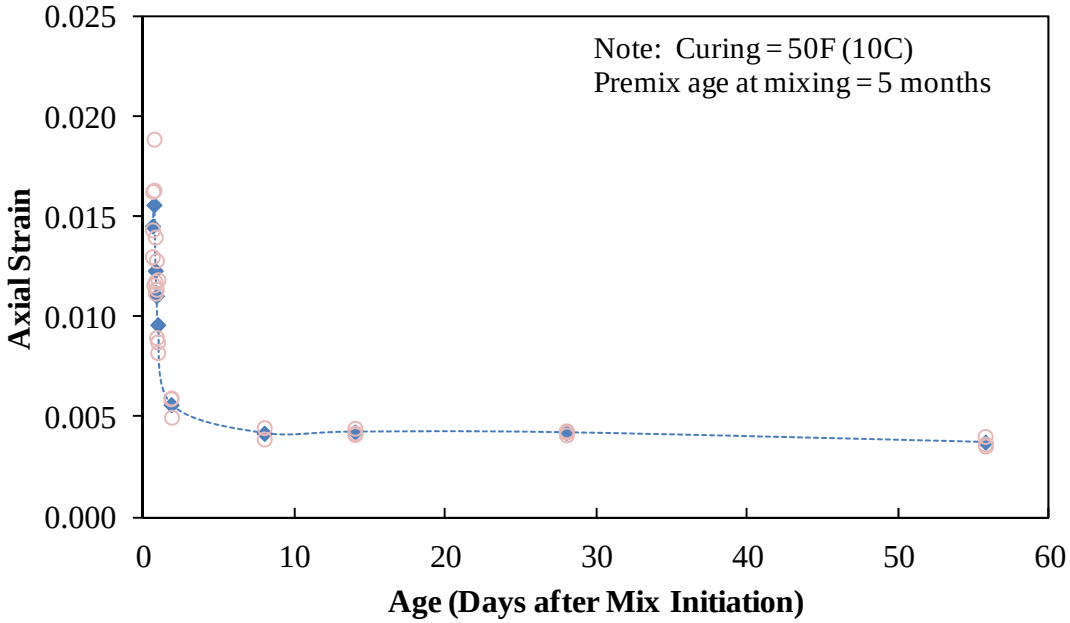

Figure 19. Graph. Strain at peak stress curve for batch SG2.

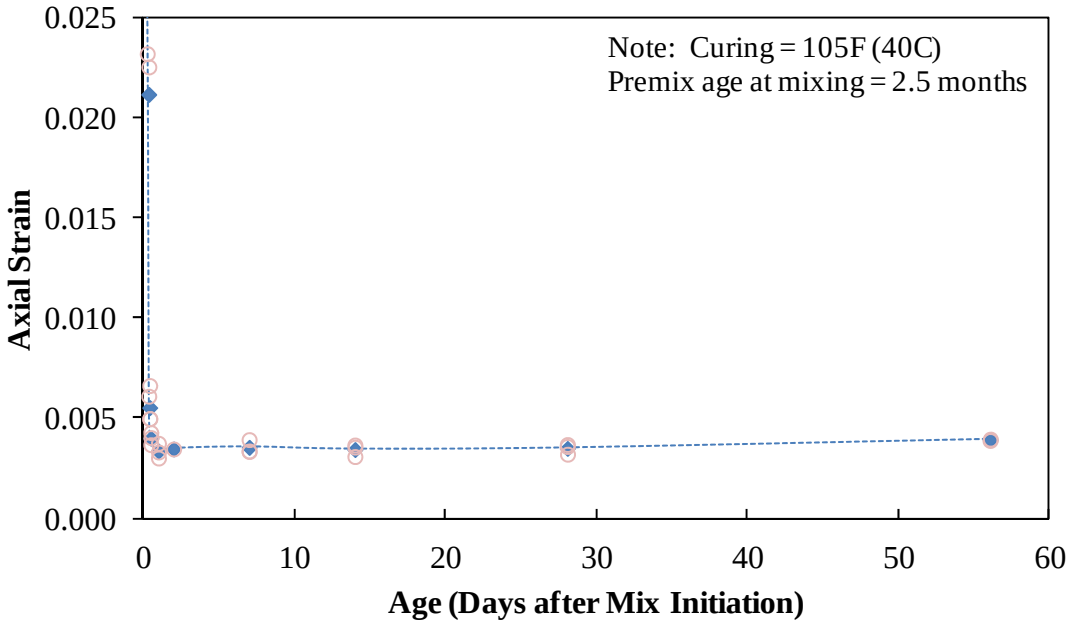

Figure 20. Graph. Strain at peak stress curve for batch SG3.

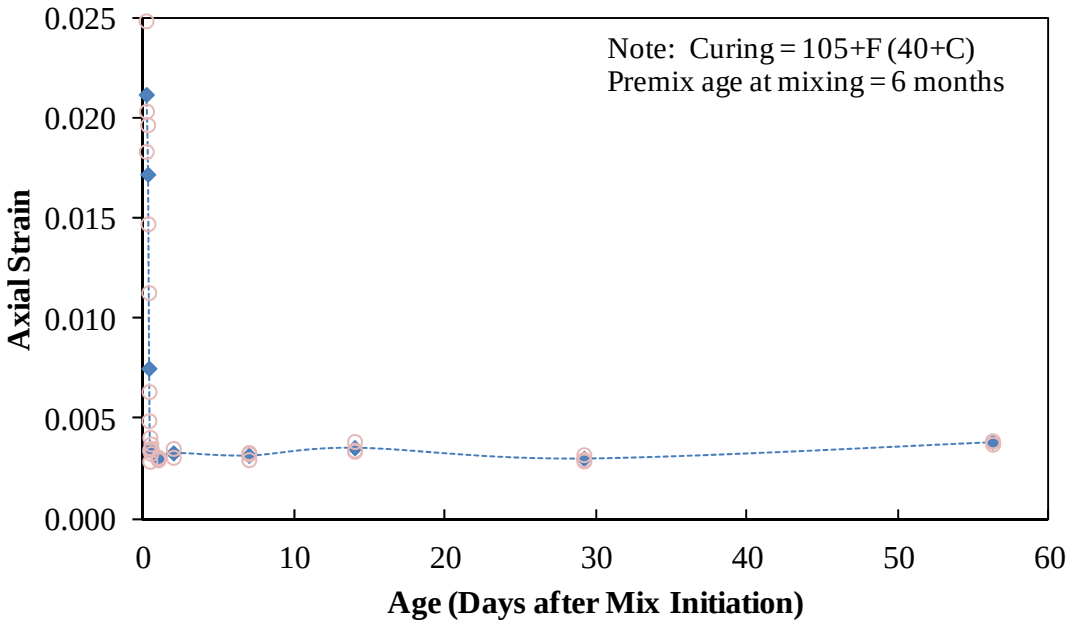

Figure 21. Graph. Strain at peak stress curve for batch SG4.

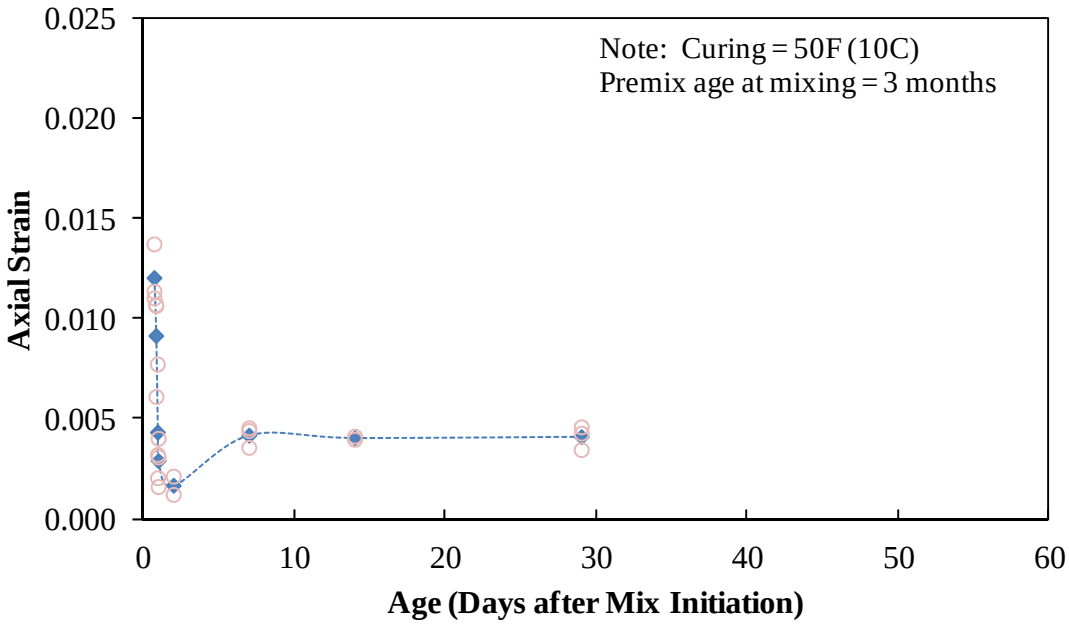

Figure 22. Graph. Strain at peak stress curve for batch SG5.

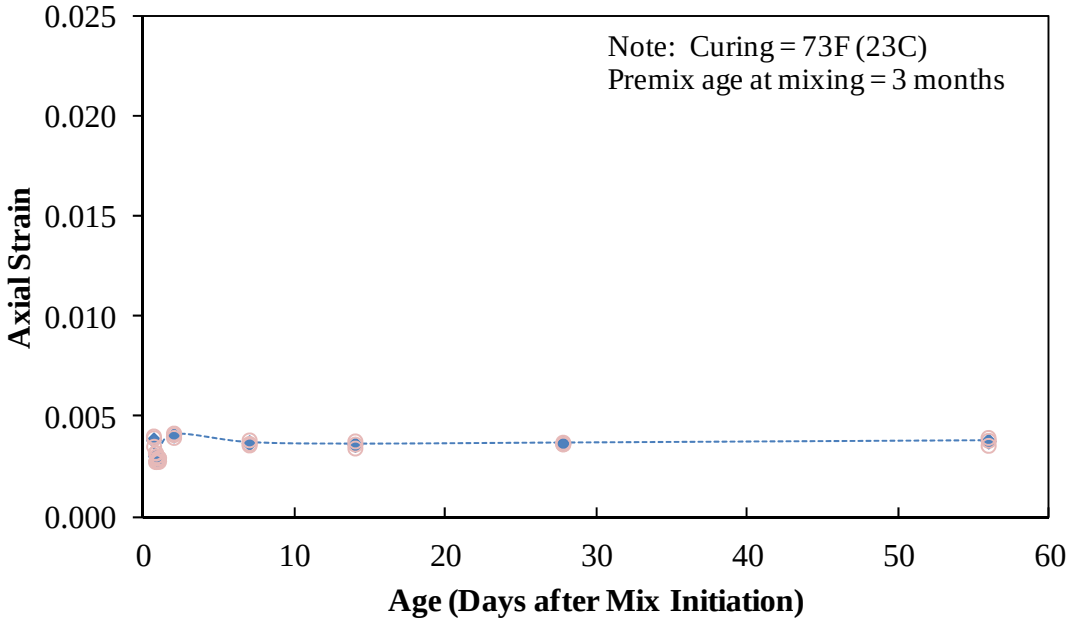

Figure 23. Graph. Strain at peak stress curve for batch SG6.

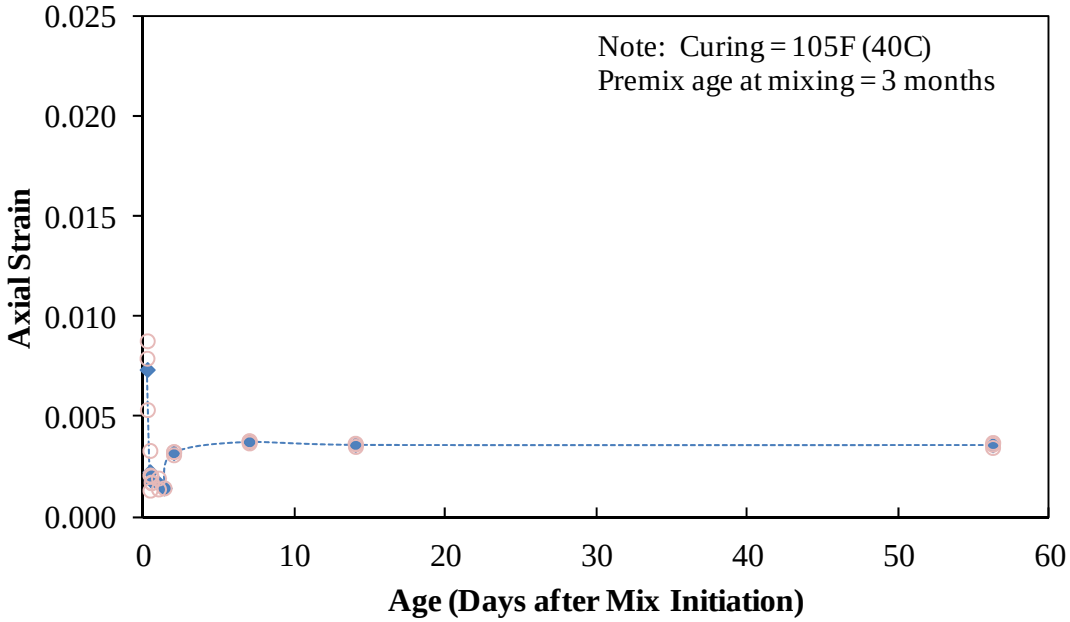

Figure 24. Graph. Strain at peak stress curve for batch SG7.

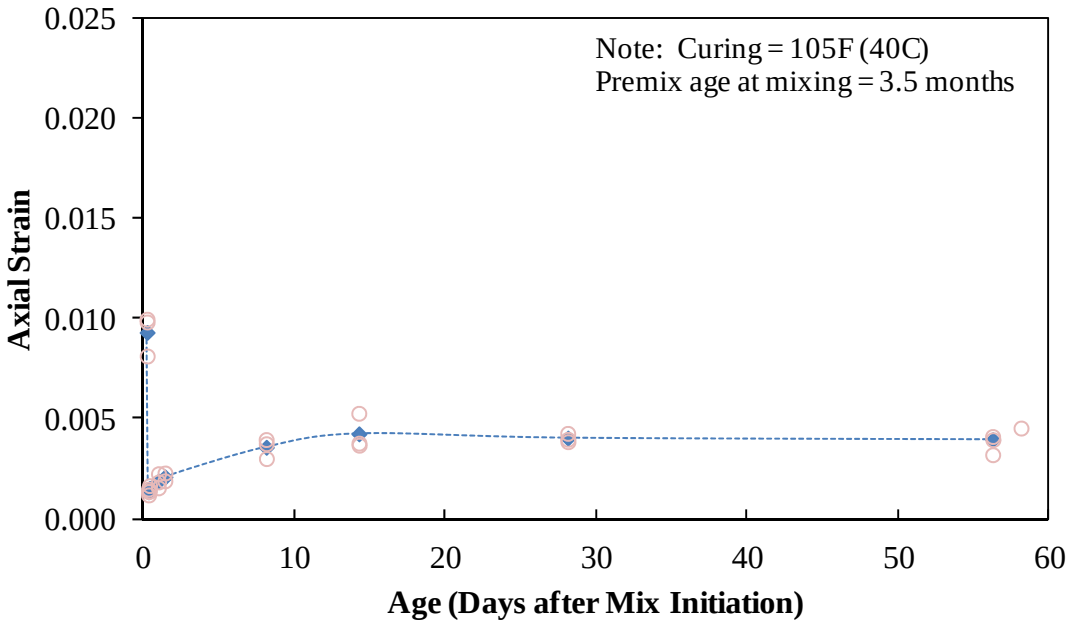

Figure 25. Graph. Strain at peak stress curve for batch SG8.

COMPRESSIVE STRESS-STRAIN RESPONSE

Another representation of the compressive mechanical response in relation to the parameters investigated is provided by graphing curve families. Figure 26 through Figure 33 provide the stress-strain results for each batch of test specimens, with representative samples from a variety of test ages shown for each batch. These families of curves depict the full stress-strain curve for a single test specimen at the designated ages. It is generally assumed that with each subsequent test age, the curve will exhibit increased stiffness and strength. Although specimens were tested at many ages, only the ages common to all eight batches have been graphed.

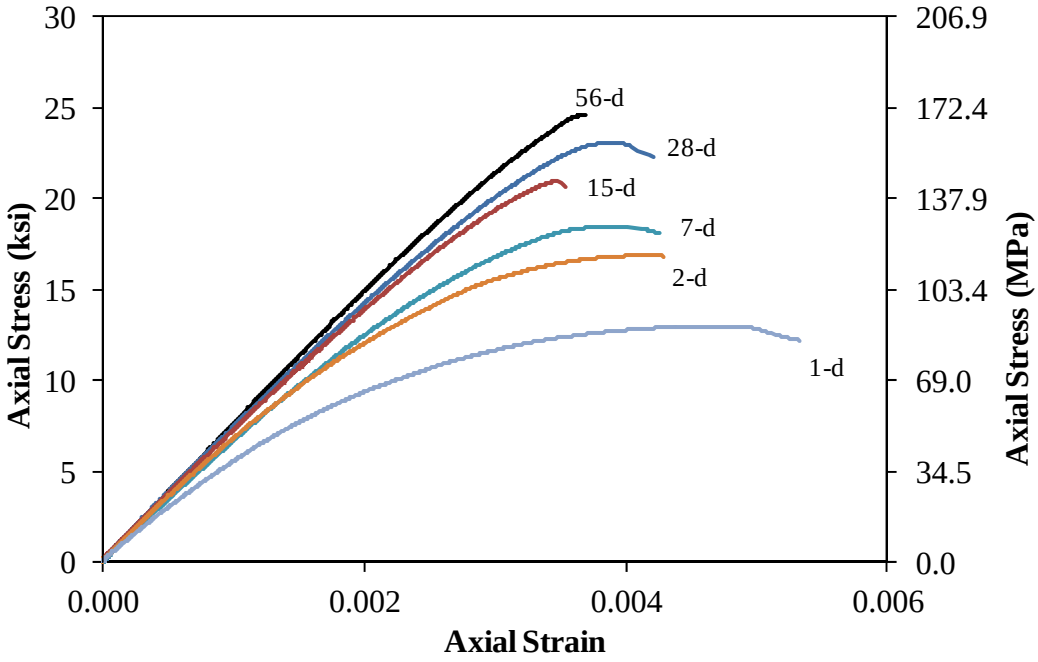

Figure 26. Graph. Stress-strain response for batch SG1.

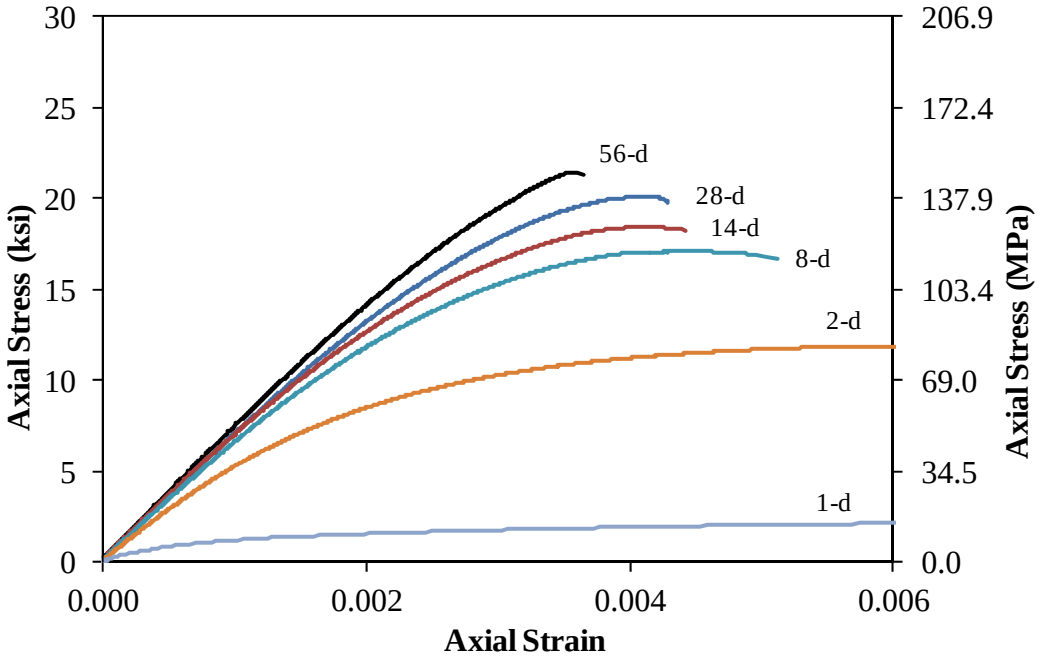

Figure 27. Graph. Stress-strain response for batch SG2.

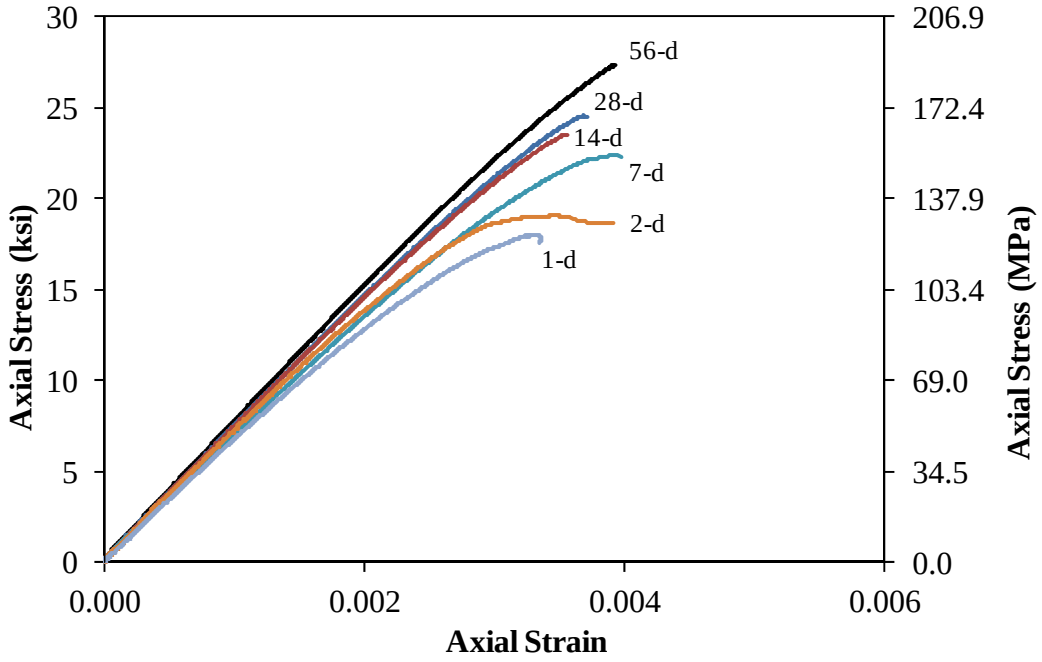

Figure 28. Graph. Stress-strain response for batch SG3.

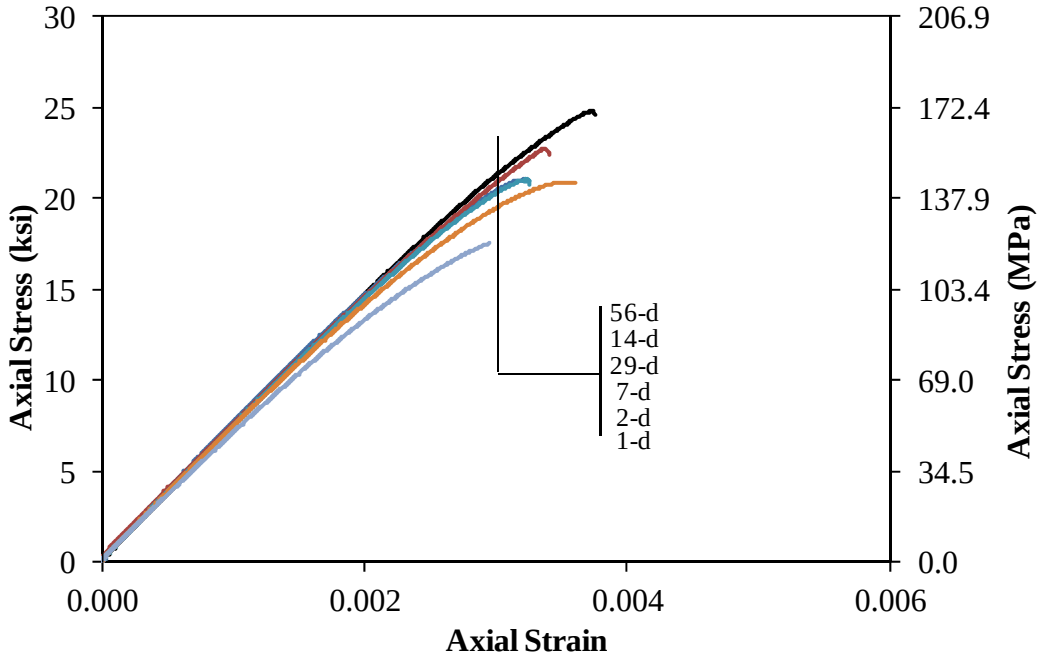

Figure 29. Graph. Stress-strain response for batch SG4.

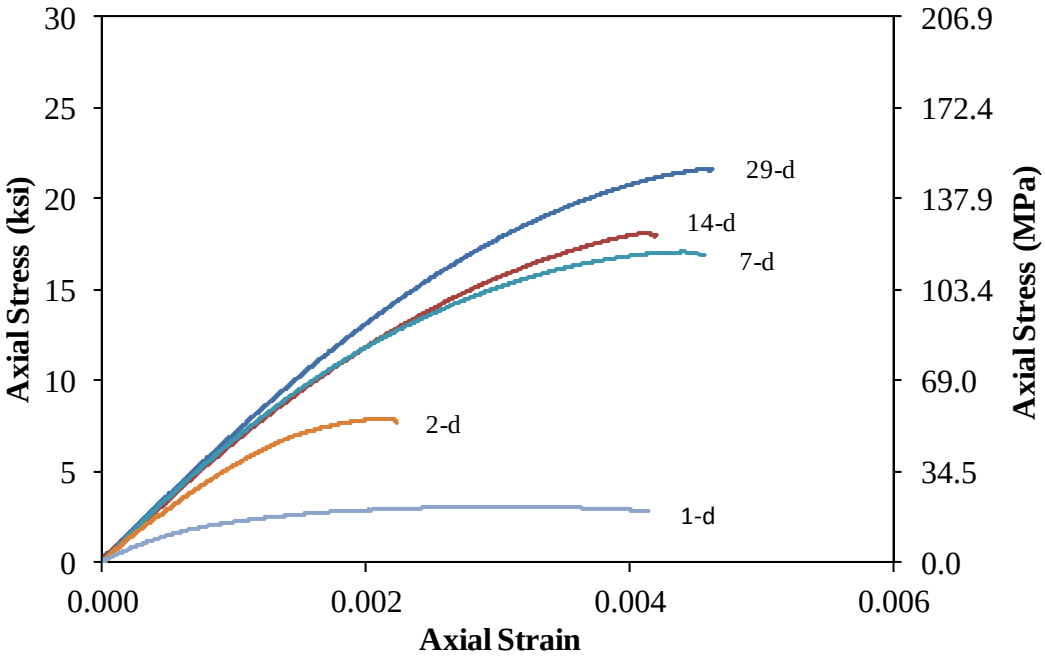

Figure 30. Graph. Stress-strain response for batch SG5.

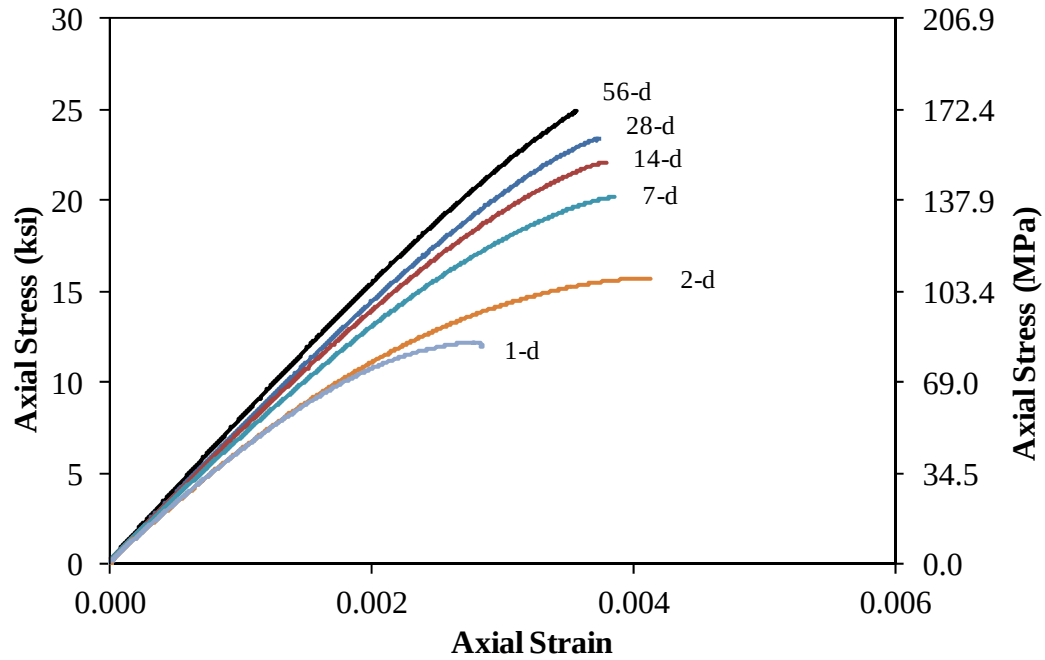

Figure 31. Graph. Stress-strain response for batch SG6.

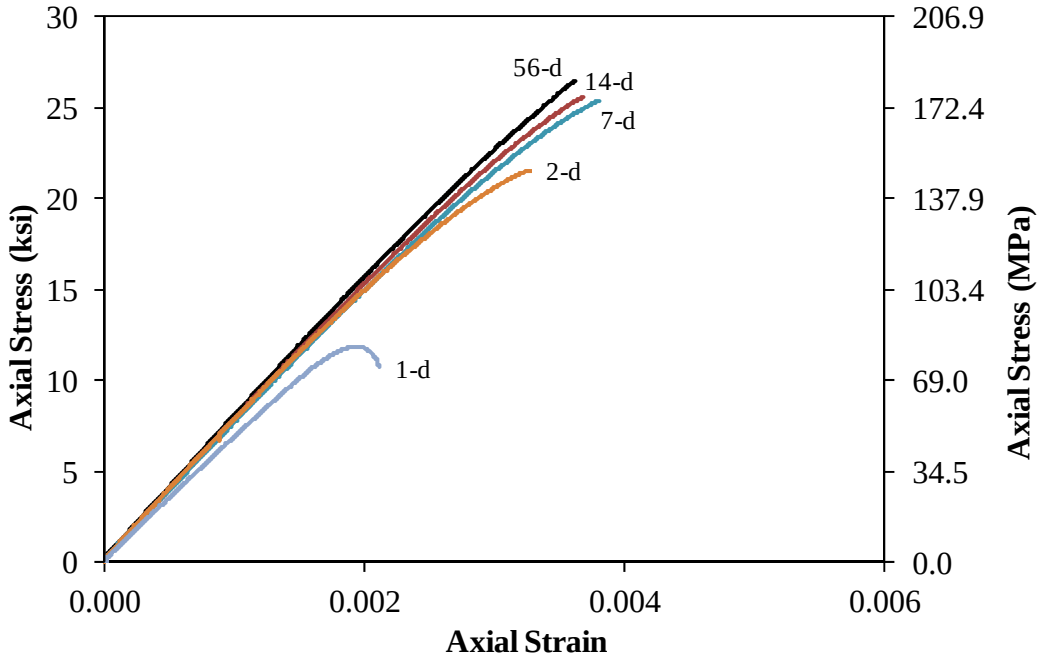

Figure 32. Graph. Stress-strain response for batch SG7.

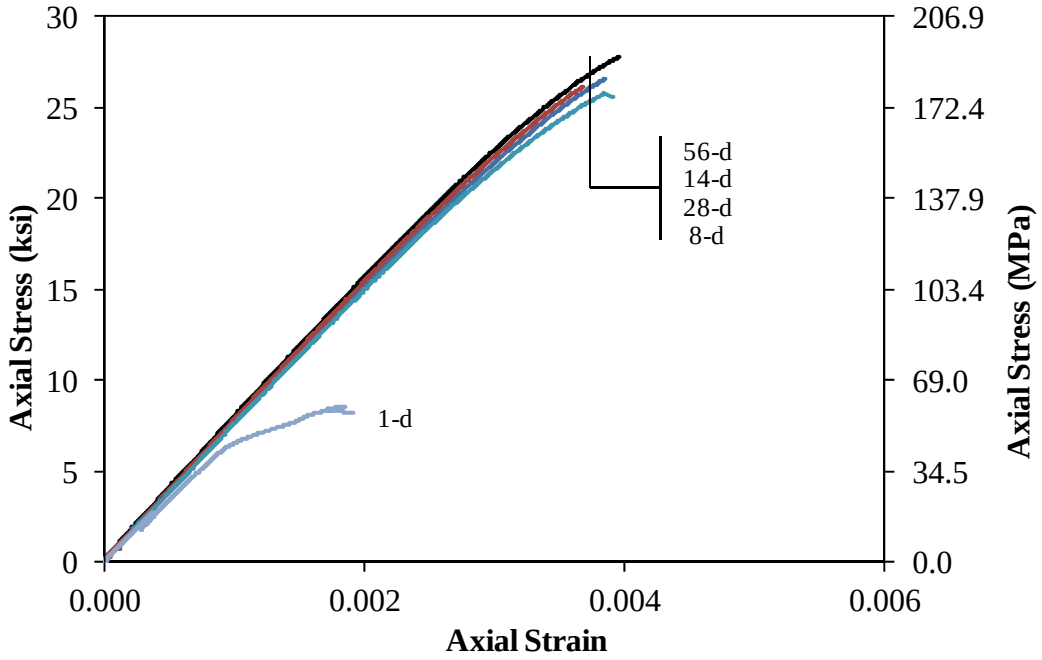

Figure 33. Graph. Stress-strain response for batch SG8.

CHAPTER 5. DISCUSSION OF RESULTS

INTRODUCTION

Analysis of the compressive mechanical test results are presented in this chapter. Specifically, peak compressive strength, modulus of elasticity, and strain results will be discussed. Additionally, the rate of strength gain with respect to time and under varied curing conditions will be compared. Finally, relationships between test parameters will be constructed and discussed.

COMPRESSIVE STRENGTH DEVELOPMENT WITH TIME

The rate of compressive strength gain can be a critical performance indicator which determines the appropriateness of a concrete for the application under consideration. UHPC-class concretes have been recognized to express a dormant period with limited compressive strength for some hours after mix initiation and subsequent placement. Also, these same concretes tend to express rapid strength gain once the retardation of the cementitious reactions has diminished. The results presented in Chapter 4 from batches SG1 through SG6 are compiled here so as to provide a relationship between the time after mix initiation, the curing temperature, and the compressive strength. Results from batches SG7 and SG8 are not presented here due to the discontinuous strength gain behavior expressed by those batches.

Figure 34 presents the compressive strength versus time after mix initiation results for each specimen from batches SG1 through SG6. In order to more clearly show the early age behaviors, the plot presents the timeframe from mix initiation through 9 days. Figure 35 presents similar results from mix initiation through 56 days after mix initiation. The dotted lines provide a qualitative indication of the average response observed for each pair of batches at each curing temperature. From these results, it is clear that the curing temperature plays a significant role in the time to initiation of strength gain, the rate of strength gain, and the time to attainment of various strength levels. Note that time to strength initiation of strength gain is defined as the time at which compressive mechanical strength begins to rapidly develop.

A regression analysis was completed on the test results from each of the three curing temperature regimes. The analysis stipulated that a single equation relate the compressive strength, $f'_{c,t}$, to the time after mix initiation, *t*, through the applied curing temperature, *T*. The Weibull Cumulative function has previously been demonstrated to relate the time and compressive strength[3], so it was engaged again here in this analysis. The shape of this function appropriately captures the shape of the strength gain curve from the initiation of rapid strength gain through the plateau near the ultimate compressive strength. It does not capture the initial strength gain behaviors wherein the response begins to transition into exhibiting comparatively small values.

Based on this function and the experimental results, the time to initiation of rapid strength gain was estimated. For the 105°F (41°C), 73°F (23°C), and 50°F (10°C) curing regimes, the time to rapid strength gain initiation was estimated to be 0.43 days, 0.58 days, and 0.88 days, respectively. For constant curing temperatures within this range the equation in Figure 36 can be used to estimate the time to initiation of strength gain based on the curing temperature.

The full equation for the strength gain versus time is presented in Figure 37. The constants relevant to each of the three curing temperature regimes are presented in Table 14. The three curves are plotted in Figure 38. The curves can be observed to appropriately fit the data while also imitating the conceptual response which occurs as concrete gains strength.

This UHPC formulation is observed to be capable of gaining strength very rapidly, with the higher curing temperature significantly accelerating the strength gain. The batches with 105°F (40°C) curing temperatures reached 14 ksi (96.5 MPa) approximately 14 hours after mix initiation. The batches with 73°F (23°C) curing temperatures reached 14 ksi (96.5 MPa) approximately 29 hours after mix initiation. The batches with 50°F (10°C) curing temperatures reached 14 ksi (96.5 MPa) approximately 5 days after mix initiation.

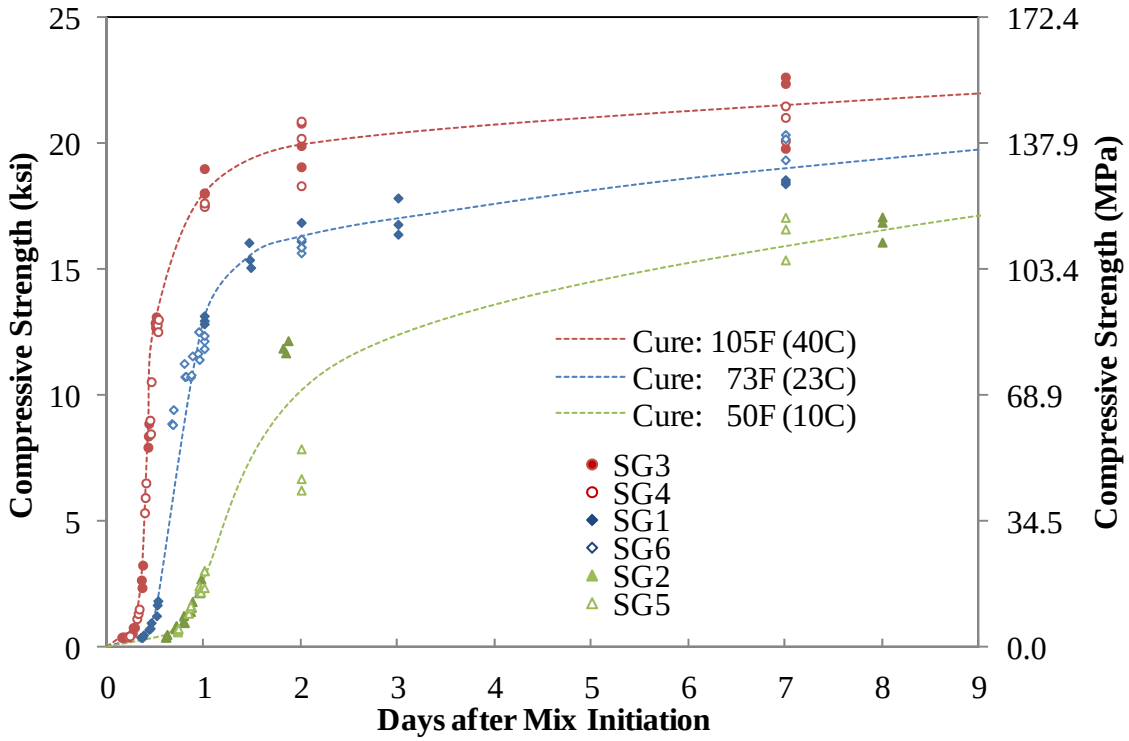

Figure 34. Graph. Early-age compressive strength gain results.

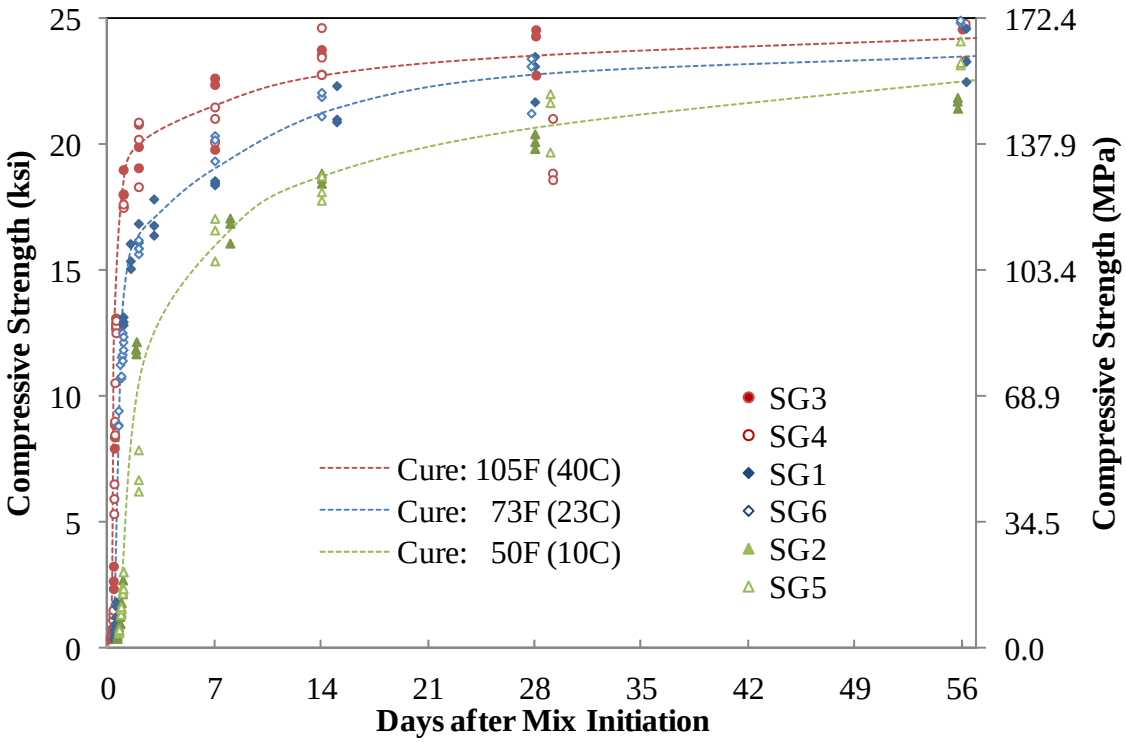

Figure 35. Graph. Compressive strength results through 56 days after mix initiation.

$$t_{start} = \frac{2.8}{\sqrt{T}}$$

with: t_{start} as the time of initiation of strength gain in days, and

T as the curing temperature in Celsius.

Figure 36. Equation. Relationship between curing temperature and initiation of rapid compressive strength gain.

$$f'_{c,t} = f'_{c,28d}\left(1 - e^{-\left(\frac{t-\frac{2.8}{\sqrt{T}}}{a}\right)^{b}}\right)$$

with: $f'_{c,28d}$ as the compressive strength at 28 days,

$f'_{c,t}$ as the compressive strength at time t in days after mix initiation,

T as the curing temperature in Celsius,

a as a fitting parameter in days, and

b as a dimensionless fitting parameter.

Figure 37. Equation. Relationship between time after mix initiation and compressive strength as a function of curing temperature.

Table 14. Parameters relevant to function presented in Figure 37.

Curing Regime	$\boldsymbol{T}$ (Celsius)	$f'_{c,28d}$ (ksi)	$\boldsymbol{a}$ (days)	$\boldsymbol{b}$
105°F (41°C)	41	24.5	0.25	0.25
73°F (23°C)	23	24	1.0	0.30
50°F (10°C)	10	22.5	4.0	0.50

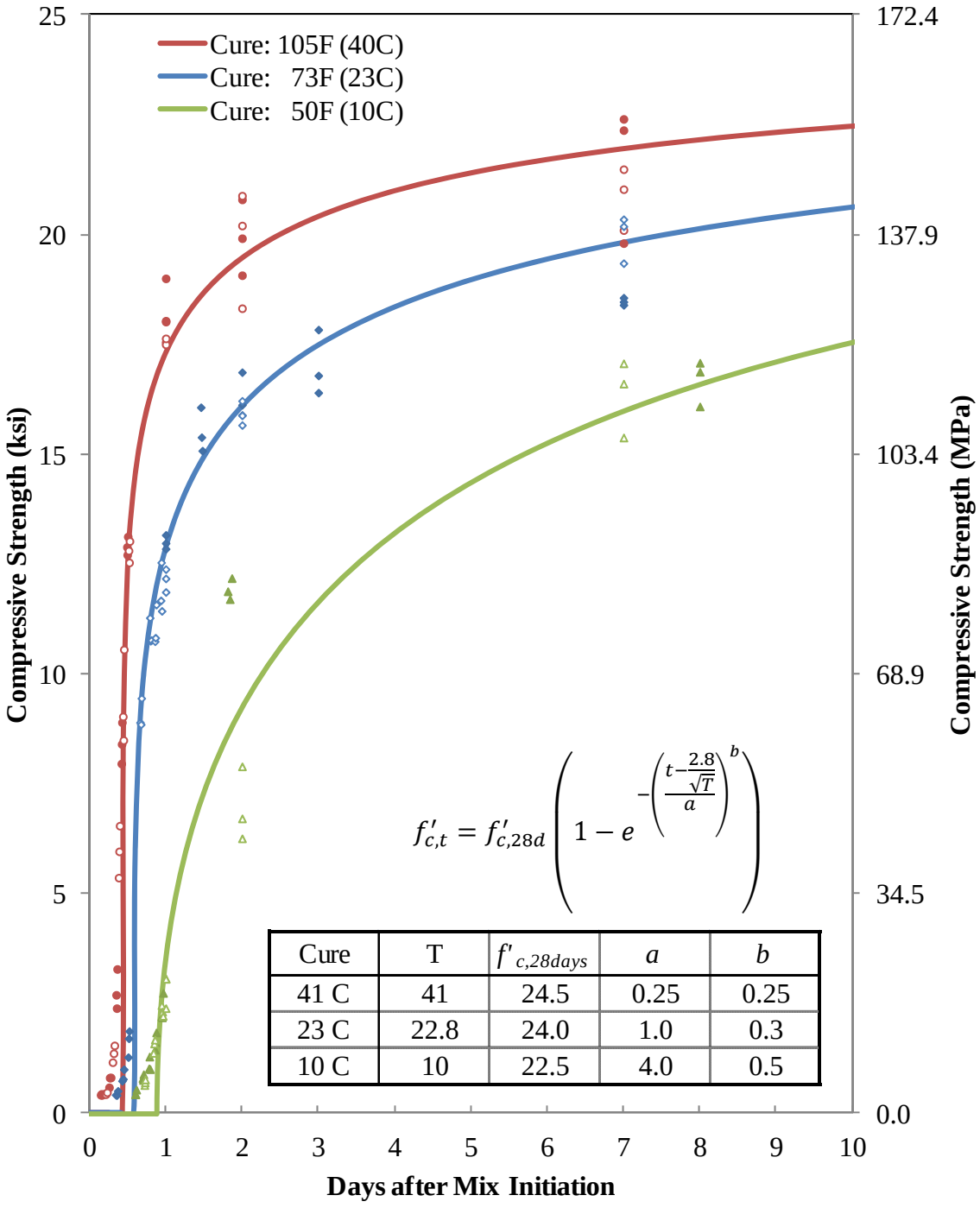

Figure 38. Graph. Compressive strength results with associated best-fit curves.

STRENGTH GAIN RESPONSE OF CHEMICALLY-ACCELERATED MIXES

The responses observed from batches SG7 and SG8 provide an indication of the performance of this UHPC-RS when used in conjunction with a particular chemical accelerator. Consideration of the results revealed a key feature of these mixes. As mentioned previously, the use of this product was suggested as a means to accelerate the attainment of high early-age strengths. In the two mixtures that included the CNI in their proportions, the compressive mechanical response during the first 5 days after mix initiation exhibited a unique behavior dissimilar from the other non-chemically accelerated batches. The curves of both SG7 and SG8 distinctly show an intermediate hold occurring in the compressive strength gain at approximately two days after mix initiation. By 14 days after mix initiation, this early age behavior seems to have been elapsed and the strength versus time response for these specimens surpasses those that did not contain the CNI. Because the applications of UHPC-RS may emanate from a need for rapid strength gain (i.e. closure pours, roadway repairs requiring traffic delays/rerouting), careful study of the impact of this or other chemical admixtures should be completed prior to deployment.

It should also be noted that, although CNI contributed to inconsistencies in the early data, the response at 7 days and beyond was greater than comparable responses observed from mixtures that did not contain CNI. For instance, at 7 days, the average peak compressive strength for CNI mixtures was 24.6 ksi (170 MPa), while the highest average mechanical response of any other mixture at 7 days was batch SG3 at 21.6 ksi (150.7 MPa). SG3, SG7, and SG8 were all subjected to the 105°F (40°C) curing regime. The strength curves for batches containing CNI exhibited less strength increase from 7 to 56 days compared with either of the other curing regimes; however, the average compressive strength values for CNI batches were still greater than the other batches at test ages of 7, 14, 28, and 56 days.

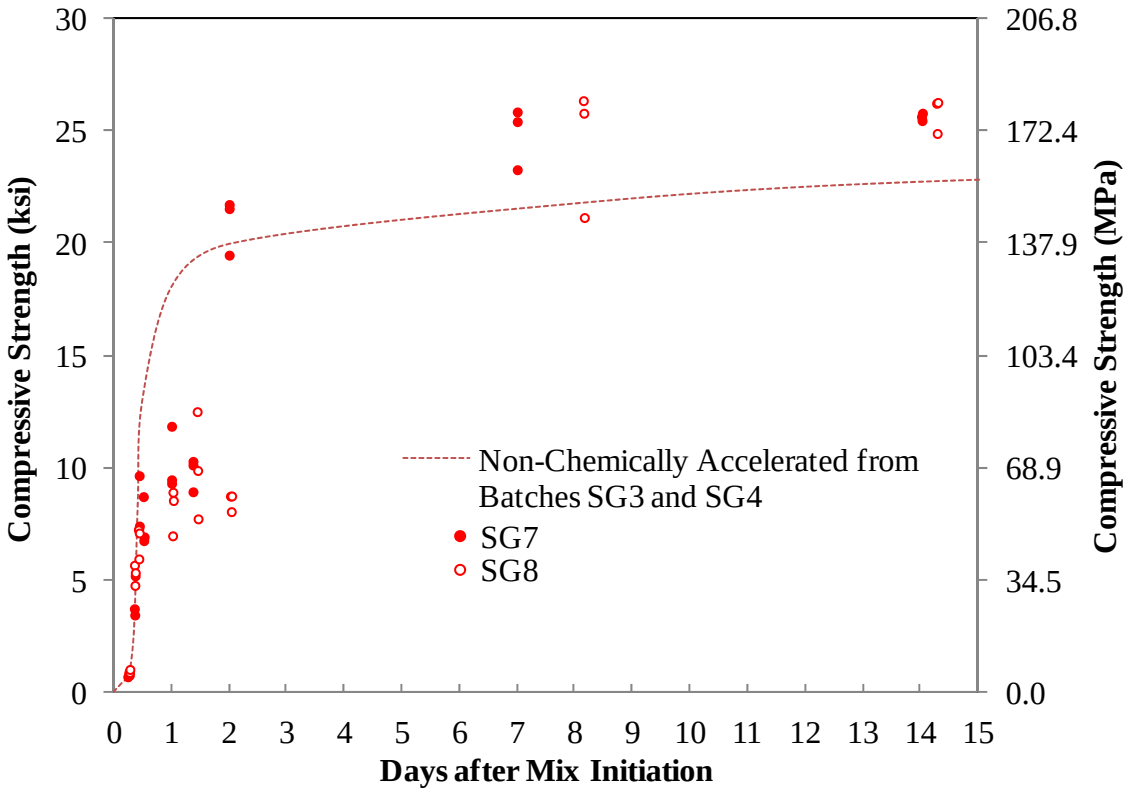

Figure 39. Graph. Compressive strength results for batches SG7 and SG8 through 15 days after mix initiation.

MODULUS OF ELASTICITY DEVELOPMENT WITH TIME

Similar to the compressive strength gain results, the modulus of elasticity results were compiled together in order to assess the impact of the curing temperatures on the modulus of elasticity growth with time. Figure 40 presents the results through 9 days after mix initiation and Figure 41 presents the results through 56 days. Results from batches SG1 through SG6 are compiled here, while batches SG7 and SG8 are not presented here due to the discontinuous strength gain behavior expressed by those batches. The dotted lines in the figures provide a qualitative indication of the average response observed for each pair of batches at each curing temperature. From these results, it is clear that the curing temperature plays a significant role in the time to initiation of stiffness gain, the rate of stiffness gain, and the time to attainment of various stiffness levels.

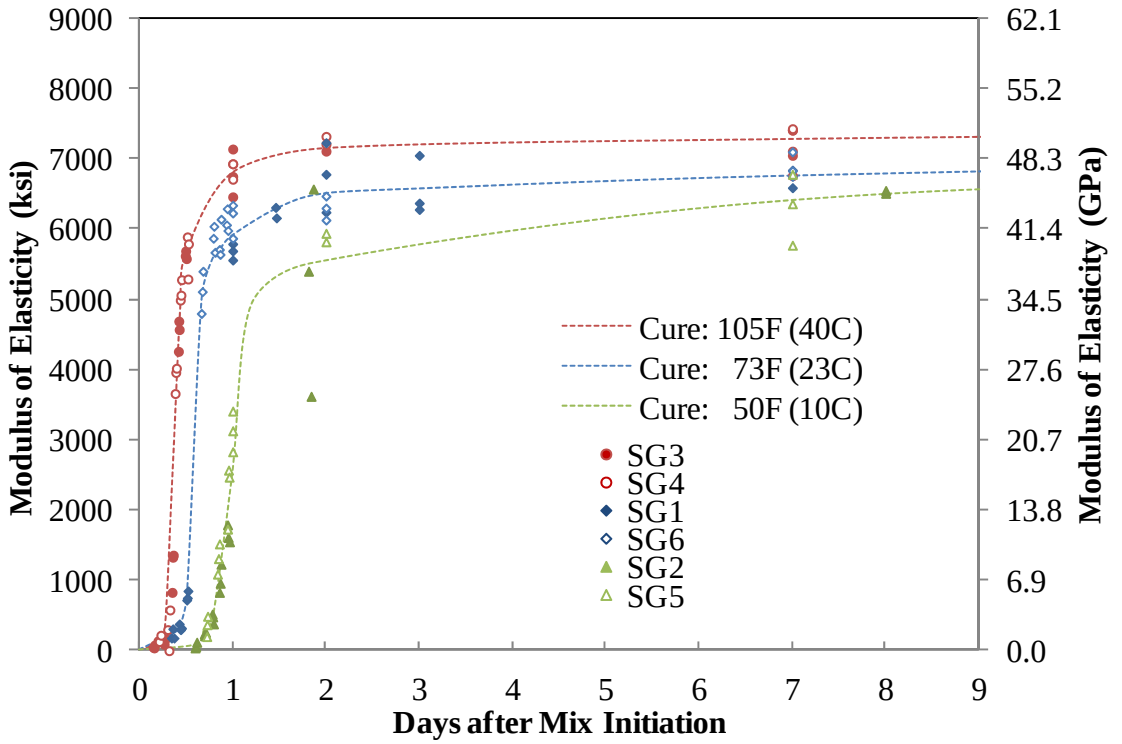

Figure 40. Graph. Modulus of elasticity results through 9 days after mix initiation.

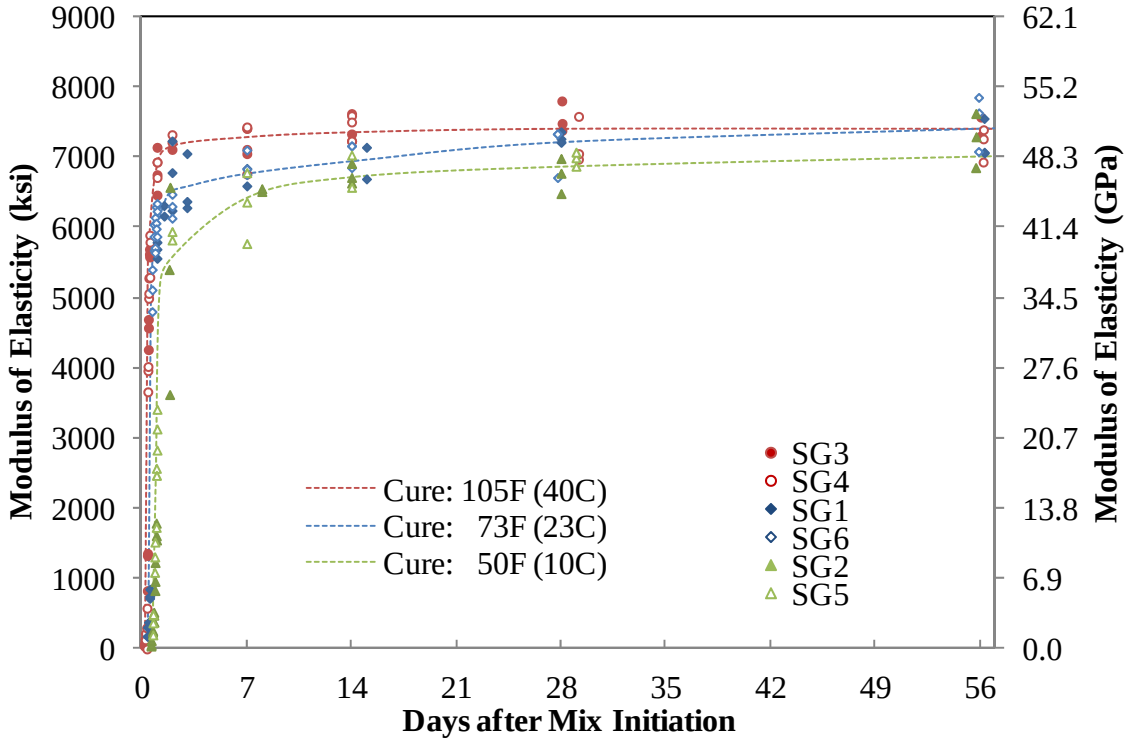

Figure 41. Graph. Modulus of elasticity results through 56 days after mix initiation.

STRAIN AT PEAK COMPRESSIVE STRENGTH

Similar to the compressive strength gain and modulus of elasticity gain results, the strain at peak compressive strength results were compiled to assess the impact of curing temperature on the strain at peak stress resistance. Figure 42 presents the results through 7 days after mix initiation and Figure 43 presents the results through 56 days. Results from batches SG1 through SG6 are compiled here, while batches SG7 and SG8 are not presented here due to the discontinuous strength gain behavior expressed by those batches. The dotted lines in the figures provide an indication of the average response observed for each pair of batches at each curing temperature. As previously discussed, the curing regime is again demonstrated to play a significant role in the development of mechanical properties.

The results indicate that by two days after mix initiation, specimens from all three curing temperature regimes have stabilized to a nearly constant strain value. The 105°F (40°C) curing regime specimens stabilized at approximately 0.0035, while the 73°F (23°C) and 50°F (10°C) specimens stabilized at approximately 0.0037 and 0.0041, respectively. By 56 days after mixing initiation, the observed strains were approximately 0.0036, 0.0038, and 0.0041 for the 105°F (40°C), 73°F (23°C), and 50°F (10°C) specimens, respectively.

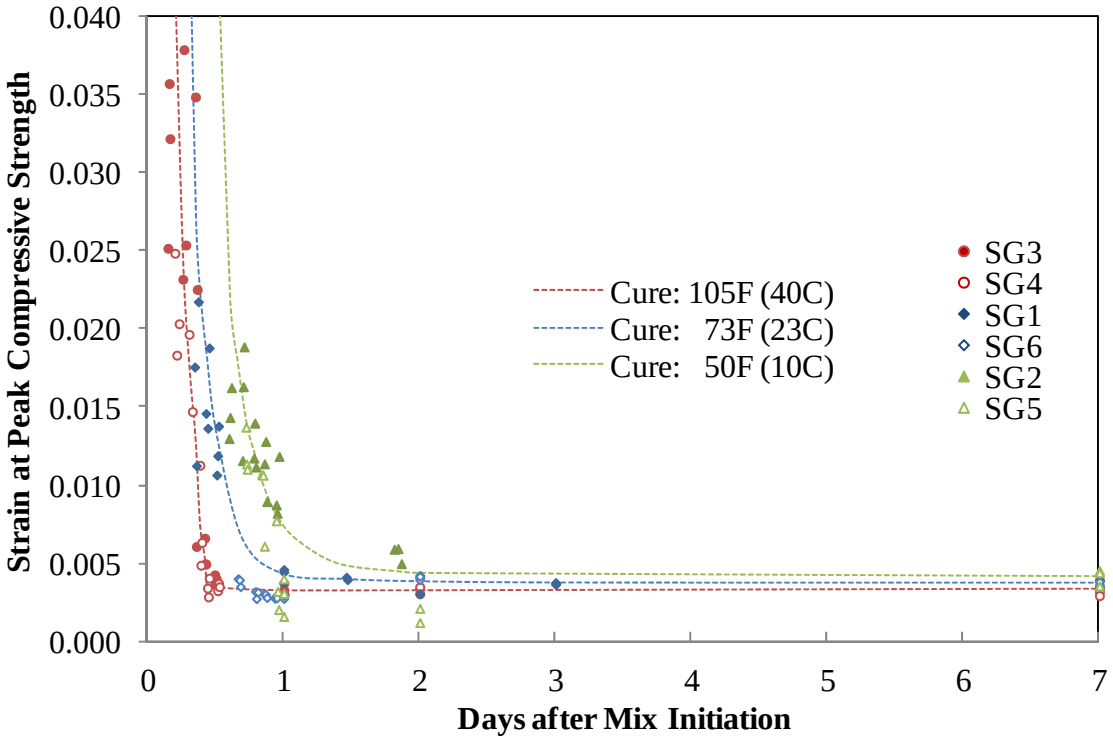

Figure 42. Graph. Strain at peak compressive strength results through 7 days after mix initiation.

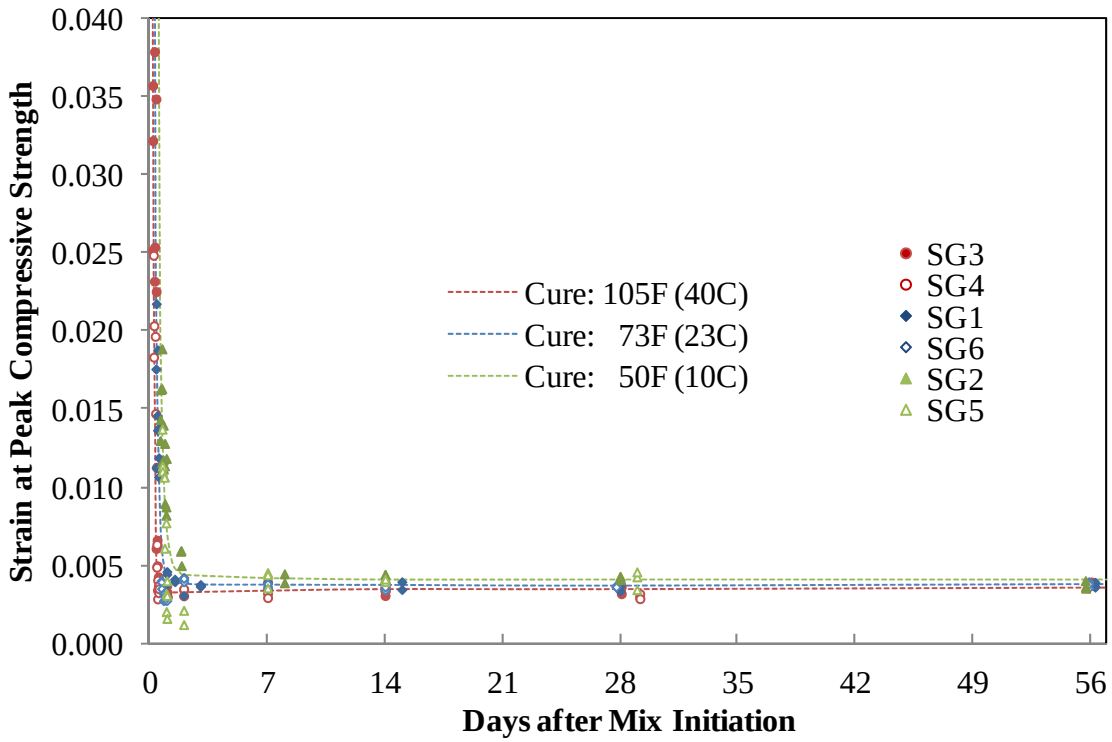

Figure 43. Graph. Strain at peak compressive strength results through 56 days after mix initiation.

MODULUS OF ELASTICITY AS A FUNCTION OF COMPRESSIVE STRENGTH

The modulus of elasticity and the compressive strength of concrete have long been associated with one another. Many testing programs have investigated the relationship between these fundamental concrete properties, frequently resulting in the recommendation of a relationship wherein the modulus of elasticity is expressed as a function of a constant multiplied by the compressive strength raised to a fractional power.

The American Concrete Institute's Building Code and Commentary (ACI 318) provides two relationships for the modulus of elasticity.[9] The equation in Figure 44 shows the first relationship wherein the square root of the compressive strength of concrete is related to the modulus of elasticity through a scalar factor. In this equation, both the compressive strength, f_c', and the modulus of elasticity, E_c, are in psi. This equation was derived from and is most relevant to normal strength and normal weight concrete.

$$E_c = 57000\sqrt{f_c'}$$

Figure 44. Equation. ACI 318 approximation of modulus of elasticity.

ACI 318 provides a second relationship for the modulus of elasticity wherein the unit weight of the concrete is included. This modification allows for estimation of the modulus of elasticity for concrete with a unit weight between 90 and 155 lb/ft^3 (1,440 and 2,480 kg/m^3). This modification

of the estimation equation is important, because both the weight of the concrete and the modulus of elasticity are normally heavily dependent on the type of coarse aggregate used. The equation in Figure 45 presents this relationship in U.S customary units, with ρ as the unit weight of concrete in lb/ft^3. Recall that the unit weight of the UHPC studied herein is approximately 155 lb/ft^3 (2,480 kg/m^3). Using this unit weight, this equation would transform into an equation similar to the one in Figure 44 with a scalar of 63,700. Note that the equation shown in Figure 45 is also the relationship provided in the AASHTO Load and Resistance Factor Design (LRFD) Bridge Design Specification.[10]

$$E_c = 33\rho^{1.5}\sqrt{f_c'}$$

Figure 45. Equation. ACI 318 approximation of modulus of elasticity including density.

ACI 363 presents a relationship between the compressive strength and the modulus of elasticity that was developed specifically for high strength concretes.[11] In particular, this relationship was developed for concretes up to 12 ksi (83 MPa). It is shown in Figure 46.

$$E_c = 40000\sqrt{f_c'} + 1000000$$

Figure 46. Equation. ACI 363 approximation for modulus of elasticity.

Prior research on UHPC mechanical properties conducted within the FHWA Structural Concrete Research Program developed a relationship specifically applicable to a commonly available UHPC.[4] This equation, shown in Figure 47, follows the form of the ACI 318 equation in Figure 44 while using a different coefficient.

$$E_c = 46200\sqrt{f_c'}$$

Figure 47. Equation. Graybeal (2007) approximation for UHPC modulus of elasticity.

At compressive strengths below 8 ksi (55 MPa), the equation proposed in Figure 47 was found to overestimate the modulus of elasticity. The equation provided in Figure 48 was proposed as providing a better fit to the observed response.[4] The primary applicability of this equation is during the early strength gain portion of the response during which UHPC-class materials are not commonly subjected to structural loadings.

$$E_c = 7100000e^{\left[-\frac{1}{2}\left(\frac{ln\left(\frac{f_c'}{44000}\right)}{1.7}\right)^2\right]}$$

Figure 48. Equation. Graybeal (2007) approximation for UHPC modulus of elasticity during initial compressive strength gain.

The relationships in Figure 47 and Figure 48 were developed based on physical testing of UHPC cylinders according to the test procedure engaged in the present study. In addition to the data on which these equations are based,[3] additional tests have been completed on the same UHPC formulation as part of other research efforts within the FHWA Structural Concrete Research Program. Some of these tests are associated with the results presented in (12), while others are associated with the research project summarized in (13). This tested UHPC formulation was procured in multiple batches between 2002 and 2010. The 275 individual data points from these studies are presented in Figure 49 along with the equations from Figure 47 and Figure 48. The equation in Figure 47 presents an appropriate fit over the compressive strength range from 8 to 35 ksi (55.2 to 241.3 MPa).

All of the modulus of elasticity versus compressive strength results developed as part of the present study are presented in Figure 50 and Figure 51. Figure 51 also includes six additional test results obtained as part of a different ongoing study at TFHRC focused on the development length of prestressing strand embedded into UHPC. All of these results were obtained from tests on the same rapid strengthening formulation of UHPC. The tested formulation was obtained in multiple batches in 2011 and 2012.

Figure 51 also presents the relationships presented in Figure 47 and Figure 48. The Figure 47 equation clearly underestimates the modulus of elasticity within the compressive strength range of greatest relevance to the use of this UHPC. To address this shortcoming, the coefficient of the relationship has been modified, and the equation shown in Figure 52 is proposed. Over the compressive strength range from 14 to 26 ksi (96.5 to 179.3 MPa), this equation presents an appropriate fit to the 116 individual data points.

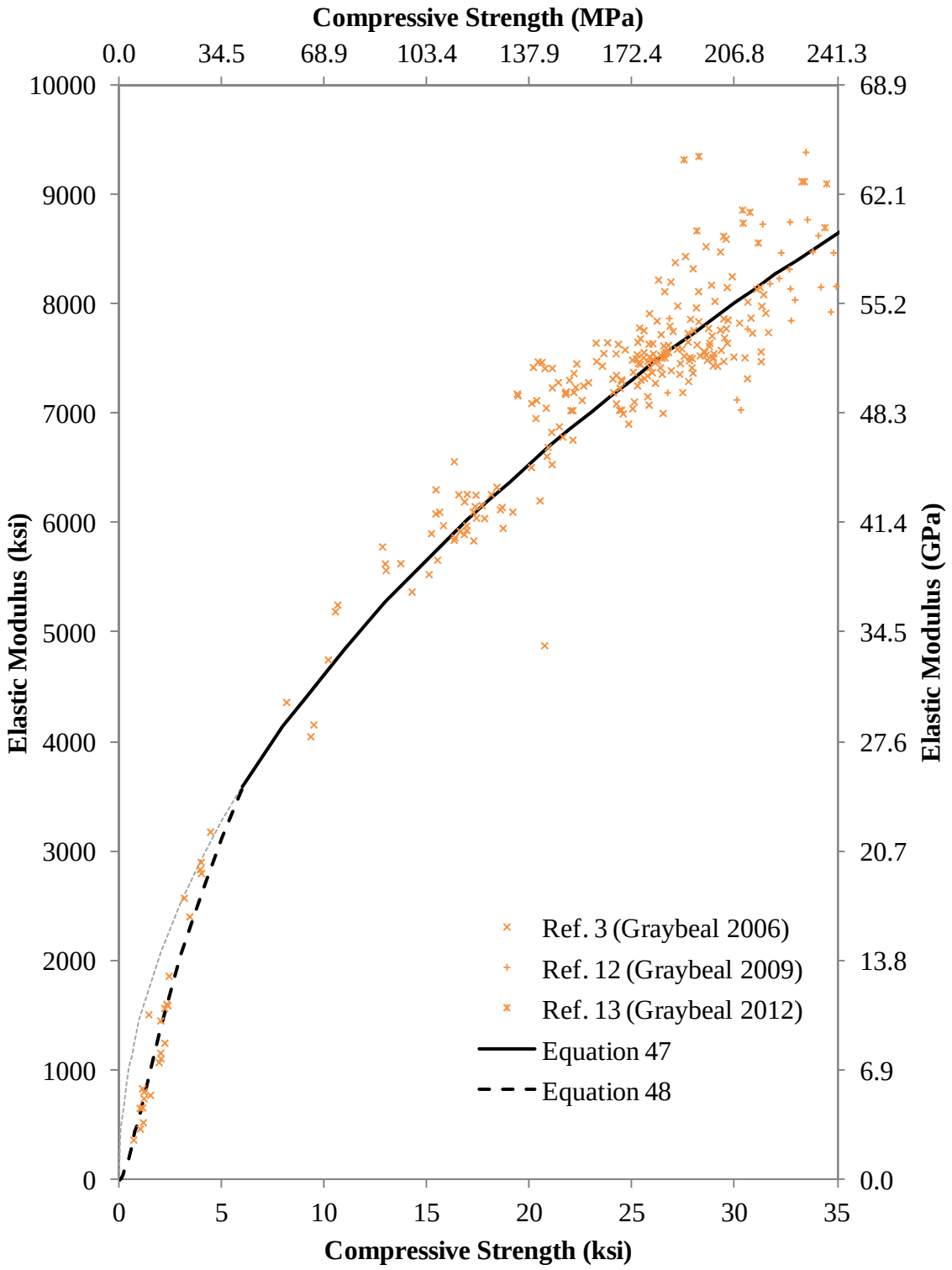

Figure 49. Graph. Modulus of elasticity results as a function of compressive strength generated through prior FHWA UHPC research.

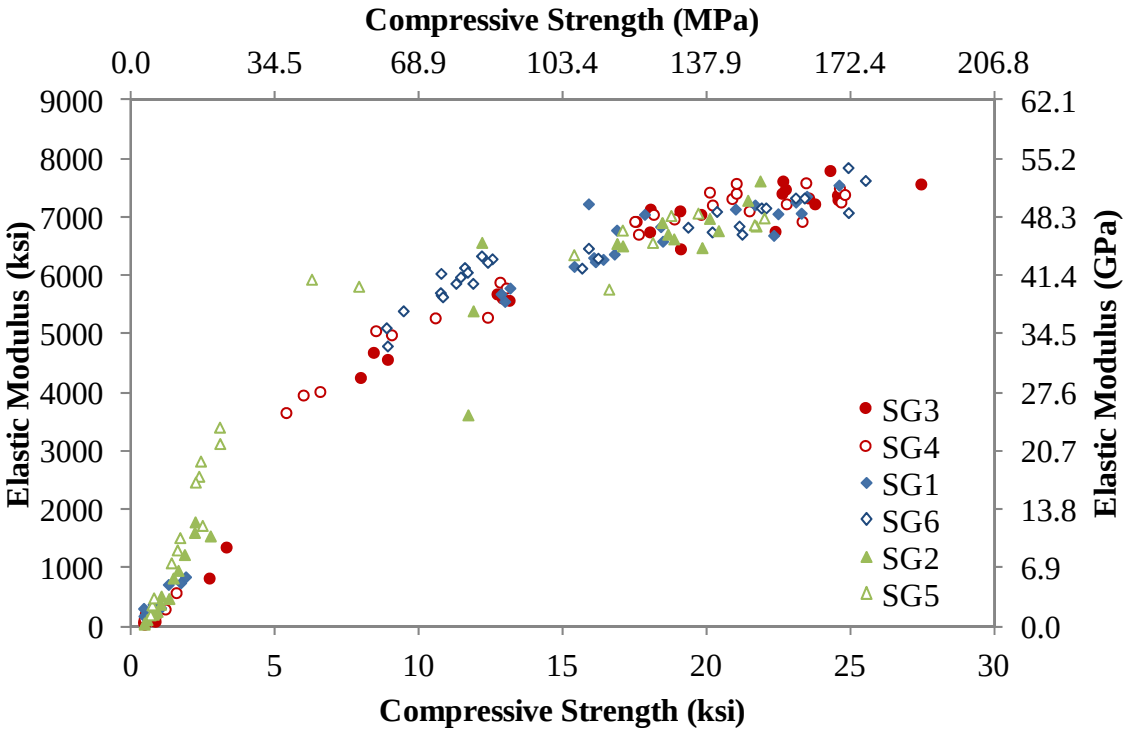

Figure 50. Graph. Modulus of elasticity results as a function of compressive strength from the present study.

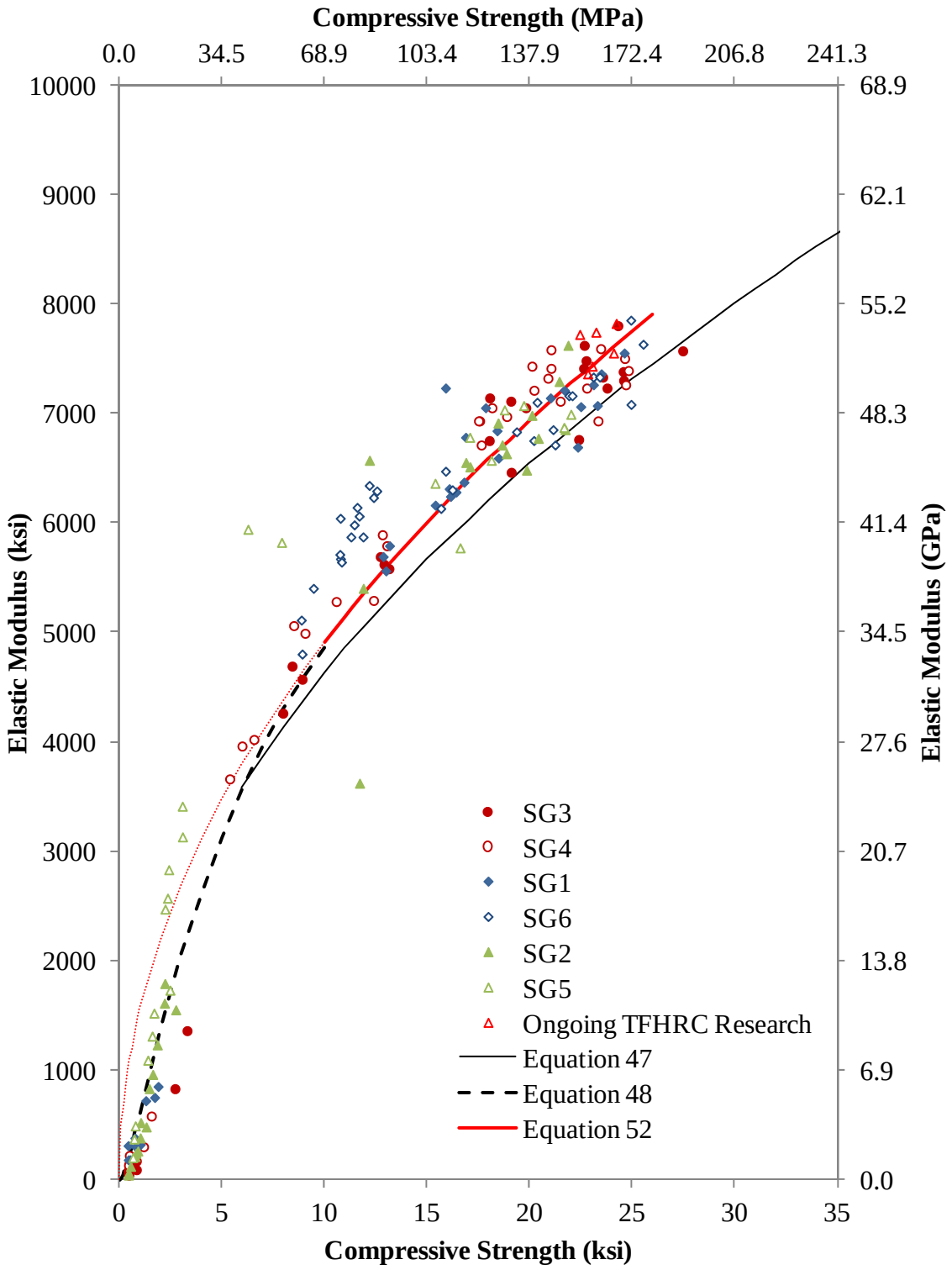

Figure 51. Graph. Modulus of elasticity results as a function of compressive strength including proposed predictive equation.

$$E_c = 49000\sqrt{f_c'}$$

Figure 52. Equation. Proposed modulus of elasticity relationship for UHPC-RS formulation.

EFFECT OF PREMIX BLEND AGE ON STRENGTH GAIN

Given the fine powders contained within a UHPC premix, it may be expected that the age of the constituents at the time of water addition and mixing might impact the rate of occurrence of the chemical reactions within mixed the concrete. This would be due to the natural tendency for finely ground powders to agglomerate thus reducing their exposed surface area. In this study, the tested UHPC mixes ranged in age at mixing from approximately 2.5 to 6 months after the initial blending of the premix. An older and a younger batch were tested for each of the three curing regimes.

Within the premix age range investigated, no clear indication of reaction deceleration was observed for the older age batches.

LINEARITY OF COMPRESSIVE RESPONSE

As concrete is subjected to high compressive stresses, it is commonly assumed that the concrete begins to develop internal microcracking and an associated reduction in stiffness. As reported in previous studies of UHPC, this type of concrete can exhibit a more linear compressive stress-strain response than is normally associated with concrete.[3,4] The data collected in this study allows for a determination of the linearity of the response.

The linearity of the response captured for each test specimen was analyzed in terms of the stress decrease observed relative to the stress value which would occur in a linear-elastic response. This concept is illustrated in Figure 53, wherein the stress-strain response from a specimen in the SG2 batch is displayed. The linear-elastic response is shown along with an indicator of the strain, ε_c, where the stress, f_c, was observed to be 10% below the linear-elastic response. The magnitude of the stress decrease is indicated with the variable α. In this case, when the specimen exhibited a stress of 15.5 ksi (107 MPa), that stress level was 10% below the linear-elastic stress as determined by an extension of the tangent modulus of elasticity, E_c.

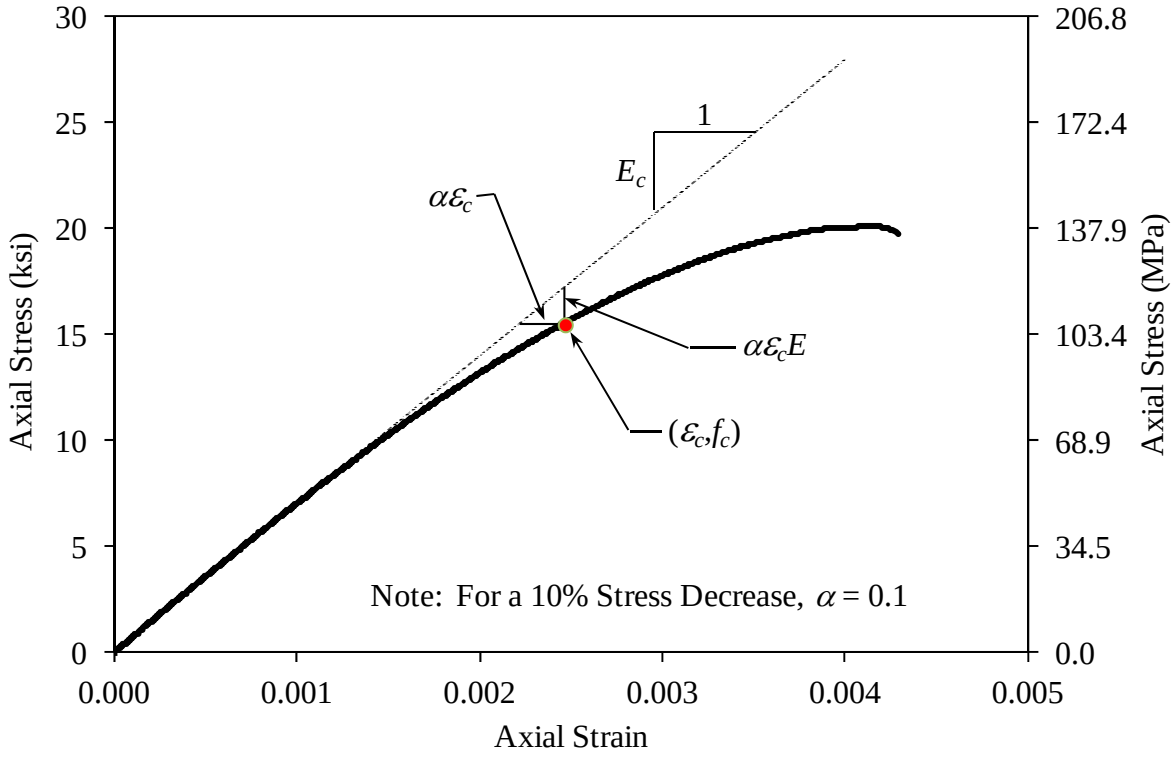

Figure 53. Illustration. Linearity of compressive stress-strain response as compared to linear-elastic behavior.

The responses of specimen sets SG1 through SG6 were analyzed to determine the linearity of the compressive stress-strain response. The results in terms of the stress at which the stress was 10% below the corresponding linear-elastic stress level are presented in Figure 54. For sets SG3 and SG4 which were subjected to the elevated temperature curing, the UHPC was demonstrated to achieve at least 80% of its compressive strength while remaining within 10% of its linear-elastic response at compressive strength levels above approximately 15 ksi (103 MPa). For sets SG1 and SG6 which were subjected to the ambient room temperature curing, the UHPC was demonstrated to achieve at least 75% of its compressive strength while remaining within 10% of its linear-elastic response at compressive strength levels above approximately 18 ksi (124 MPa). For sets SG2 and SG5 which were subjected to the cold temperature curing, the UHPC was demonstrated to achieve at least 70% of its compressive strength while remaining within 10% of its linear-elastic response at compressive strength levels above approximately 20 ksi (138 MPa).

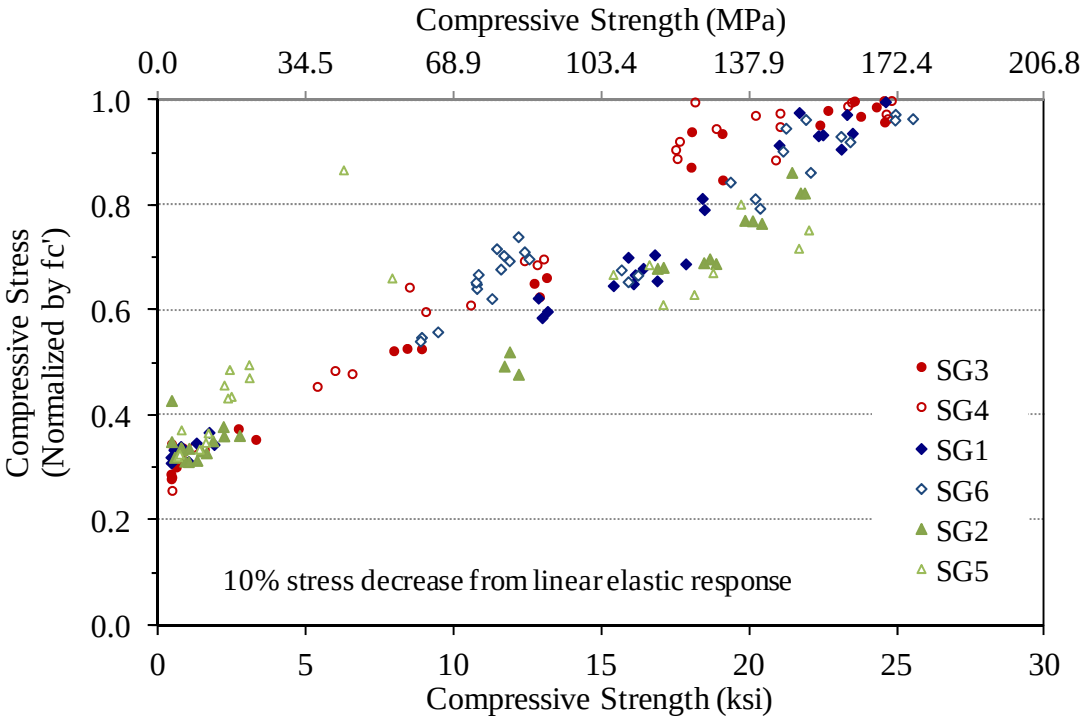

Figure 54. Graph. Compressive stress at 10% stress decrease from linear elastic response.

This method of assessing the compressive stress-strain response was implemented throughout the stress-strain responses of each specimen. As such, the overall compressive stress-strain response of the UHPC under each of the three curing regimes can be assessed. The process implemented herein is similar to that described in references (3) and (4). The stress decrease benchmarks of 1%, 3%, 5%, and 10% were captured for each specimen. Only specimens exhibiting compressive strengths above 14 ksi (96.5 MPa) were included. In order to eliminate potential inaccuracies associated with the determination of the strain as the compressive peak is approached, data relating to compressive stresses above 98% of the specimen's compressive strength were excluded.

The full set of included data from these six batches is presented in Figure 55. Both the compressive stress and the compressive strain are normalized. Similarly, Figure 56, Figure 57, and Figure 58 present the same data for each curing condition, this time with the stress deviation from linear-elastic response plotted on the vertical axis. This presentation of data highlights the critical non-linear behaviors. The results in Figure 56, Figure 57, and Figure 58 indicate an increasing non-linearity through the 10% stress decrease level, and were found to be appropriately fit by the cubic function shown in Figure 59. The constants, *A*, in this equation were found to be 0.078, 0.104, and 0.177 for the elevated temperature, ambient room temperature, and cool temperature curing conditions, respectively.

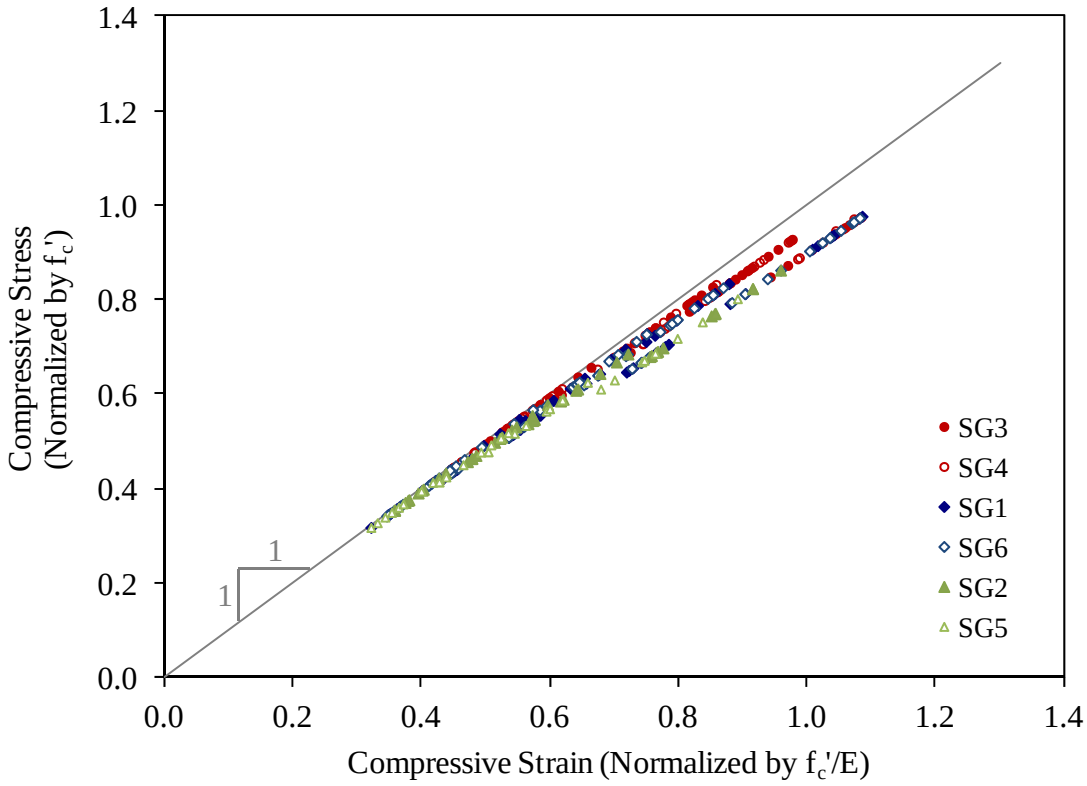

Figure 55. Graph. Normalized compressive stress-strain results.

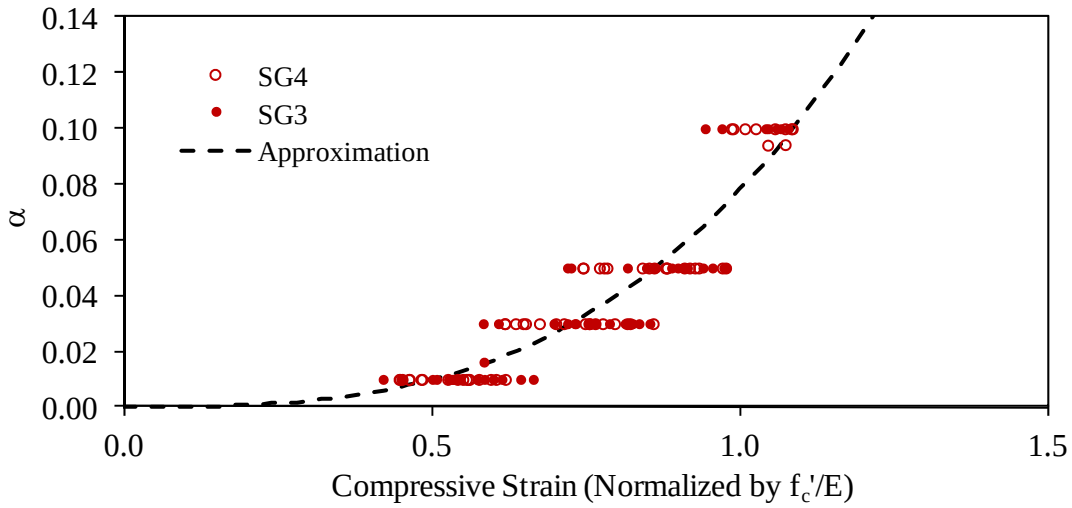

Figure 56. Graph. Deviation from linear-elastic compressive behavior for UHPC-RS cured at elevated temperature.

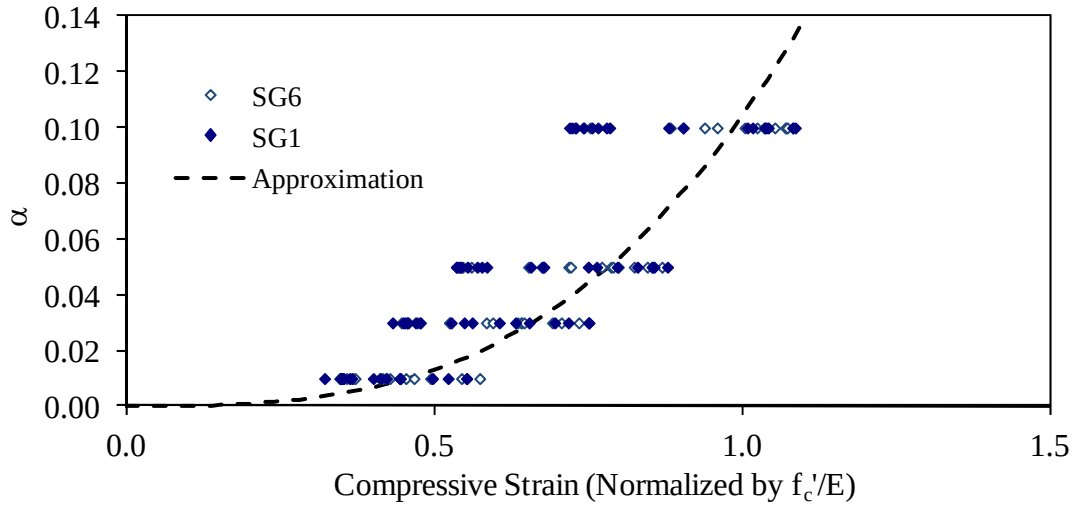

Figure 57. Graph. Deviation from linear-elastic compressive behavior for UHPC-RS cured at ambient room temperature.

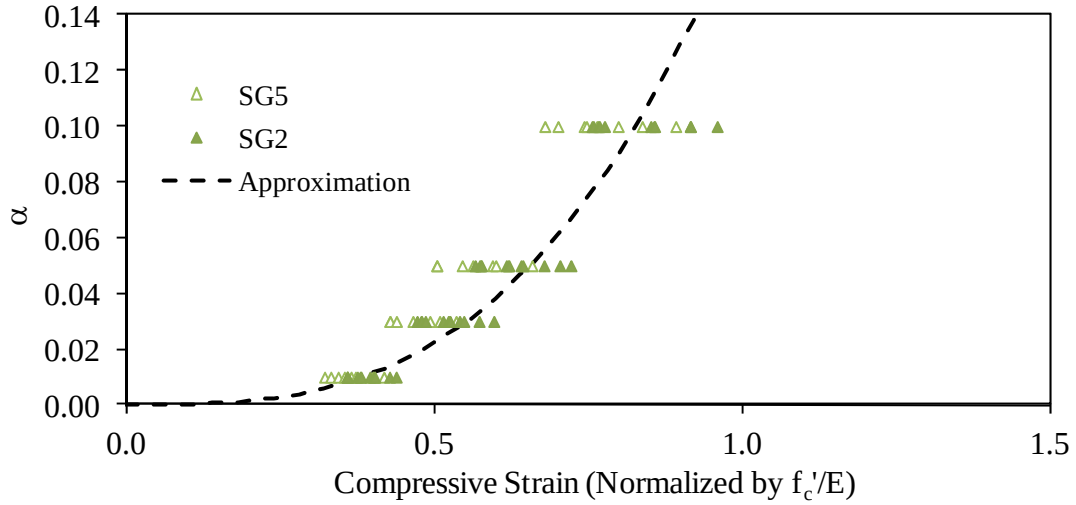

Figure 58. Graph. Deviation from linear-elastic compressive behavior for UHPC-RS cured at cool temperature.

$$\alpha = A\left(\frac{\varepsilon_c E}{f_c'}\right)^3$$

Figure 59. Equation. Deviation of compressive stress-strain response from linear-elastic behavior.

This analysis leads to a simple means for defining the ascending branch of the compressive stress-strain response of this UHPC under the three curing conditions. The equation in Figure 60 defines the compressive stress as a function of the strain, the modulus of elasticity, and the deviation from linear elastic behavior. This equation is applicable for compressive strengths above 14 ksi (96.5 MPa) and with stress decreases up to 10% from linear elastic behavior.

$$f_c = \varepsilon_c E_c (1 - \alpha)$$

Figure 60. Equation. Compressive stress-strain behavior defined as a function of the deviation from linear-elastic behavior.

The equation in Figure 60 is plotted in Figure 61 for the three curing conditions. In this example, the compressive strength is assumed to be 24 ksi (165 MPa), resulting in an assumed modulus of elasticity of 7590 ksi (52.3 GPa) based on the equation in Figure 52. Note that the responses are only plotted for the range $0 \leq \alpha \leq 0.10$.

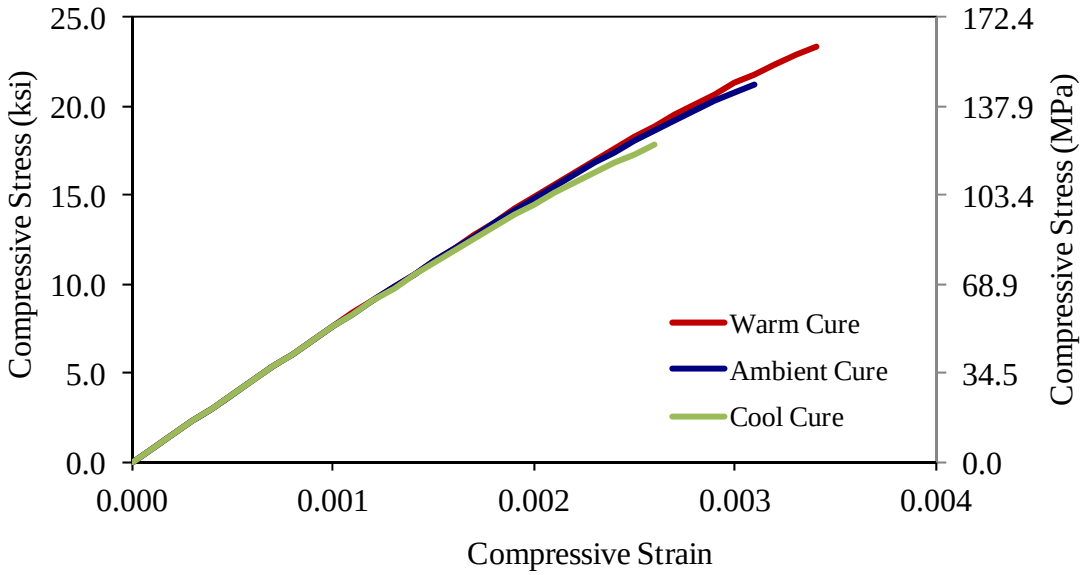

Figure 61. Graph. Compressive stress-strain response approximations for the UHPC-RS formulation tested in this study.

Overall, this linearity analysis indicates that an increase in curing temperature causes an increase in the linearity of the compressive stress-strain response. This result coincides with the results from the strain at peak compressive strength analysis, wherein the increased curing temperature resulted in a smaller strain at peak strength.

CHAPTER 6. CONCLUSIONS AND RECOMMENDATIONS

INTRODUCTION

The research discussed herein focused on observing compressive mechanical response of a rapid-strengthening UHPC, with an emphasis on assessing the impact of curing temperature, premix age at casting, and effect of a particular chemical accelerator. Conclusions, recommendations, and a possible direction for future research on related topics are presented in this chapter.

CONCLUSIONS

The following conclusions are presented based on the research presented in this report.

- The early-age compressive strength gain of this UHPC formulation is directly proportional to the curing temperature to which the UHPC is subjected. Using ambient room temperature specimens as a baseline, the cool cure specimens required significantly longer curing time to reach comparable strength levels. Similarly, specimens subjected to elevated curing temperatures achieved higher strength more quickly. All batches, regardless of curing condition, reached 56-day compressive strengths within approximately 2 ksi (13.8 MPa) of one another.
- The rate of compressive mechanical property attainment was not significantly impacted by the age of the premix at time of mix initiation. Premix ages between 2.5 and 6 months after blending were investigated.
- The use of a chemical accelerator to promote rapid strength gain in this rapid-strengthening UHPC did not seem to accelerate attainment of desired mechanical properties at early ages. After an initial rise in compressive strength during the first 24 hours, test results for both tested batches indicated a delay in additional strength gain during the following 24 hours. Later strength gain may be accelerated, with both mixtures having achieved approximately 90 percent of their 56-day compressive strengths by 7-days after casting.
- The compressive strength was found to be predictable as a function of time based on the 28-day compressive strength and the constant temperature curing regime to which the concrete is subjected.
- The modulus of elasticity of this UHPC formulation was found to be predictable as a function of the compressive strength. The developed relationship is applicable for compressive strengths from 14 to 26 ksi (96.5 to 179 MPa).
- This UHPC formulation was observed to exhibit a stress-strain response that remained closer to linear elastic behavior through a higher compressive stress than is normally expected for concrete materials. Higher curing temperatures were observed to increase the linearity of the compressive stress-strain response.

FUTURE RESEARCH

This study investigated the compressive mechanical response of a particular rapid-strengthening UHPC. Additional research on the material properties of this rapid-strengthening UHPC is in progress within the broader FHWA Structural Concrete Research Program. These studies focus

not only on compressive mechanical responses, such as uniaxial compressive strength, but also on long-term volume stability, bond strength when cast against a previously cast conventional concrete, and durability when deployed in a bridge deck.

The adoption of UHPC-RS as a conventional building material will require further research and development of properties and behaviors, in addition to consistent, documented test results. Doing so will assure the user of the performance of the final product when specified. Potential UHPC-RS research topics of interest emanating directly from this study may include the following.

- Although three curing temperatures were evaluated as part of this research, it may be valuable to investigate additional temperature ranges, including variable temperature curing regimes, which more closely mimic the conditions which might be encountered during field curing operations.
- General guidelines suggest that UHPC premix not be stored for extended periods prior to use, regardless of whether or not the premix is of the rapid-strengthening variety. Research investigating the early age mechanical properties of UHPC cast from premix older than six months could provide a fuller understanding of the impact premix age has on the overall performance of the UHPC.
- Additional tests on chemically-accelerated UHPC-RS mixtures should be conducted to determine whether there can be a significant benefit in early-age mechanical property development.
- Additional similar research on other UHPC formulations as well as other fiber reinforcements will expand the knowledge base and allow for greater understanding of the performance of this class of cementitious composite materials.

ACKNOWLEDGMENTS

The research which is the subject of this document was funded by the U.S. Federal Highway Administration. This support is gratefully acknowledged.

This research project could not have been completed were it not for the dedicated support of the federal and contract staff associated with the FHWA Structural Concrete Research Program. Special recognition goes to Dr. Jussara Tanesi who provided engineering support throughout various phases of the project, and to Bradford Tschetter who assisted with test specimen preparation and testing.

The publication of this report does not necessarily indicate approval or endorsement of the findings, opinions, conclusions, or recommendations either inferred or specifically expressed herein by the Federal Highway Administration or the United States Government.

REFERENCES

1. Graybeal, B., "Ultra-High Performance Concrete," U.S. Department of Transportation, Federal Highway Administration, FHWA-HRT-11-038, March 2011, 8 pp.

2. Graybeal, B., "Construction of Field-Cast Ultra-High Performance Concrete Connections," U.S. Department of Transportation, Federal Highway Administration, FHWA-HRT-12-038, April 2012, 8 pp.

3. Graybeal, B., "Material Property Characterization of Ultra-High Performance Concrete," Federal Highway Administration, Report No. FHWA-HRT-06-103, August 2006, 186 pp.

4. Graybeal, B.A., 2007, "Compressive Behavior of Ultra-High Performance Fiber-Reinforced Concrete," *ACI Materials Journal*, V. 104, No. 2, Mar.-Apr., pp. 146-152.

5. Graybeal, B.A., and Marshall Davis, 2008, "Cylinder or Cube: Strength Testing of 80 to 200 MPa (11.6 to 29 ksi) Ultra-High-Performance Fiber-Reinforced Concrete," *ACI Materials Journal*, V. 105, No. 6, Nov.-Dec., pp. 603-609.

6. Ahlborn, T.M., D.K. Harris, D.L. Mission, and E.J. Peuse, "Strength and Durability Characterization of Ultra-High Performance Concrete Under Variable Curing Conditions," *Proceedings, Transportation Research Board Conference*, 2011.

7. ASTM C39-11, "Standard Test Method for Compressive Strength of Cylindrical Concrete Specimens," *ASTM Book of Standards Volume 04.02*, ASTM International, West Conshohocken, PA, 2011.

8. ASTM C469-10, "Standard Test Method for Static Modulus of Elasticity and Poisson's Ratio of Concrete in Compression," *ASTM Book of Standards Volume 04.02*, ASTM International, West Conshohocken, PA, 2010.

9. ACI Committee 318, 2005, "Building Code Requirements for Structural Concrete (ACI 318-05) and Commentary (ACI 318R-05)," American Concrete Institute, Farmington Hills, MI., 430 pp.

10. AASHTO, *AASHTO LRFD Bridge Design Specifications, 6th Edition*, American Association of State Highway and Transportation Officials, 2012.

11. ACI Committee 363R, 1992, "Report on High-Strength Concrete (ACI 363R-92)," American Concrete Institute, Farmington Hills, MI., 55 pp.

12. Graybeal, B.A., 2009, "Structural Behavior of a Prototype Ultra-High Performance Concrete Pi-Girder", Report No. PB2009-115495, National Technical Information Service, Springfield, VA.

13. Graybeal, B., Baby, F., Marchand, P., Toutlemonde, F., "Direct and Flexural Tension Test Methods for Determination of the Tensile Stress-Strain Response of UHPFRC," *Proceedings, 3rd International Symposium on Ultra-High Performance Concrete*, Kassel, Germany, March 7-9, 2012, 8 pp.